Title

Thymic regulatory T cells arise via two distinct developmental programs

Journal

Nature Immunology, 20(2)

ISSN

1529-2908

Authors

Owen, David L

Mahmud, Shawn A

Sjaastad, Louisa E

et al.

Publication Date

2019-02-01

DOI

10.1038/s41590-018-0289-6

Peer reviewed

HHS Public Access

Author manuscript

Nat Immunol. Author manuscript; available in PMC 2019 July 23.

Published in final edited form as:

Nat Immunol. 2019 February ; 20(2): 195–205. doi:10.1038/s41590-018-0289-6.

Thymic regulatory T cells arise via two distinct developmental programs

David L. Owen[1], **Shawn A. Mahmud**[1], **Louisa E. Sjaastad**[1], **Jason B. Williams**[2], **Justin A. Spanier**[3], **Dimitre R. Simeonov**[4,5,6], **Roland Ruscher**[1], **Weishan Huang**[7,8], **Irina Proekt**[5], **Corey N. Miller**[5], **Can Hekim**[1], **Jonathan C. Jeschke**[2], **Praful Aggarwal**[9], **Ulrich Broeckel**[9], **Rebecca S. LaRue**[10], **Christine M. Henzler**[10], **Maria-Luisa Alegre**[11], **Mark S. Anderson**[5,12], **Avery August**[7], **Alexander Marson**[4,5,12,13,14], **Ye Zheng**[15], **Calvin B. Williams**[2], **Michael A. Farrar**[1]

[1]Center for Immunology, Masonic Cancer Center, and the Department of Laboratory Medicine and Pathology, University of Minnesota, Minneapolis, MN, 55455 USA

[2]Section of Rheumatology, Department of Pediatrics, Medical College of Wisconsin, Milwaukee, WI 53226

[3]Center for Immunology, Department of Medicine, University of Minnesota, Minneapolis, MN 55455

[4]Department of Microbiology and Immunology, University of California San Francisco, San Francisco, CA 94143

[5]Diabetes Center, University of California San Francisco, San Francisco, CA 94143

[6]Biomedical Sciences Graduate Program, University of California San Francisco, San Francisco, CA 94143, USA

[7]Department of Microbiology and Immunology, College of Veterinary Medicine, Cornell University, Ithaca, NY 14853

[8]Department of Pathobiological Sciences, School of Veterinary Medicine, Louisiana State University, Baton Rouge, LA 70803, USA

Corresponding author Michael A. Farrar (farra005@umn.edu).

Author Contributions

D.L.O. designed and conducted experiments and wrote the manuscript. S.A.M, L.E.S, J.B.W., J.A.S., D.R.S., R.R., W.H., I.P., C.N.M., C.H., J.C.J, P.A., U.B., R.S.L., C.M.H., and Y.Z. performed some experiments or analyzed data and contributed intellectually to the work. M.A., M.S.A., A.A., A.M., Y.Z., and C.B.W. provided key reagents and/or animals and intellectual contributions. M.A.F. designed experiments, supervised research, and assisted in the preparation of this manuscript. All authors read the manuscript and helped with final revisions.

Data availability statement

The data that support the findings of this study are available from the corresponding author upon request. Single-Cell RNA-Seq data is deposited at GEO with the following accession codes: GSE123067

Code availability statement

Source code for bio-informatic analyses is attached as a supplementary file.

Competing financial interests

Other authors declare no competing financial interests.

[9]Section of Genomic Pediatrics, Department of Pediatrics, Medical College of Wisconsin, Milwaukee, WI 53226

[10]Supercomputing Institute for Advanced Computational Research, University of Minnesota, Minneapolis, MN 55455

[11]Section of Rheumatology, Department of Medicine, University of Chicago, Chicago, IL 60637

[12]Department of Medicine, University of California San Francisco, San Francisco, CA 94143, USA

[13]Chan Zuckerberg Biohub, San Francisco, California 94158, USA

[14]Innovative Genomics Institute, University of California, Berkeley, CA 94720, USA

[15]Nomis Foundation Laboratories for Immunobiology and Microbial Pathogenesis, The Salk Institute for Biological Studies, La Jolla, CA 92037, USA.

Abstract

The developmental programs that generate a broad repertoire of regulatory T cells (T_{reg} cells) able to respond to both self antigens and non–self antigens remain unclear. Here we found that mature T_{reg} cells were generated through two distinct developmental programs involving $CD25^+$ T_{reg} cell progenitors ($CD25^+$ $T_{reg}P$) and $Foxp3^{lo}$ T_{reg} cell progenitors ($Foxp3^{lo}$ $T_{reg}P$). The $CD25^+$ $T_{reg}P$ had higher rates of apoptosis and interacted with thymic self-antigens with higher affinity than $Foxp3^{lo}$ $T_{reg}P$, and had a T cell antigen receptor (TCR) repertoire and transcriptome distinct from that of $Foxp3^{lo}$ $T_{reg}P$. The development of $CD25^+$ $T_{reg}P$ and $Foxp3^{lo}$ $T_{reg}P$ was controlled by distinct signaling pathways and enhancers. Transcriptomic and histocytometric data suggested that $CD25^+$ $T_{reg}P$ and $Foxp3^{lo}$ $T_{reg}P$ arose by coopting negative and positive selection programs, respectively. T_{reg} cells derived from $CD25^+$ $T_{reg}P$, but not $Foxp3^{lo}$ $T_{reg}P$, prevented experimental autoimmune encephalitis. Our findings indicate that T_{reg} cells arise through two distinct developmental programs that are both required for a comprehensive T_{reg} cell repertoire capable of establishing immune tolerance.

Regulatory T cells (T_{reg} cells) play key roles in protecting against autoimmune responses to tissues, preventing inappropriate responses to commensal organisms and dampening effector T cell responses following clearance of pathogens. However, the mechanisms that lead to the development of a population of Treg cells that can mediate such diverse functions remain unclear. T_{reg} cells were shown to develop through a two-step process in the thymus [1, 2]. The first step is driven by strong signals sent through the T cell antigen receptor (TCR), which leads to upregulation of CD25, the key component of the high-affinity receptor for IL-2, as well as the TNF receptor superfamily members GITR, OX40 and TNFR2, but not the upregulation of the transcription factor Foxp3 [1, 3]. A second, TCR-independent, step involves the conversion of the $CD25^+$ $T_{reg}P$ cells into mature $CD25^+Foxp3^+$ T_{reg} cells in a manner dependent on the cytokine IL-2 and the transcription factor STAT5 [1, 2, 4, 5]. A distinct T_{reg} cell progenitor population, characterized by low expression of Foxp3 and lacking detectable expression of CD25, was also described in the thymus [6]. This $Foxp3^{lo}$ $T_{reg}P$ cell has high expression of GITR and OX40 [3], and can differentiate into mature $CD25^+Foxp3^+$ T_{reg} cells following stimulation with IL-2 [6]. The relative contributions of these $T_{reg}P$ cell populations to the mature T_{reg} cell pool remains controversial.

Here we demonstrate that CD25$^+$Foxp3$^-$ T_{reg} cell progenitors (CD25$^+$ T_{reg}P hereafter) and CD25$^-$Foxp3^{lo} T_{reg} progenitors (Foxp3^{lo} T_{reg}P hereafter) generated mature T_{reg} cells with relatively comparable efficiency in vitro and in vivo. The two developmental pathways for T_{reg} cell generation differed in many aspects, including distinct transcriptomes and TCR repertoires. The CD25$^+$ T_{reg}P exhibited increased apoptosis, developed into mature T_{reg} cells with faster kinetics and exhibited greater reactivity with self-antigens in the thymus than Foxp3^{lo} T_{reg}P. Development of the two T_{reg} cell progenitor subsets was controlled by different cytokines, signaling pathways, gene enhancers and stromal cells in the thymus. Finally, T_{reg} cells derived from CD25$^+$ T_{reg}P, but not Foxp3^{lo} T_{reg}P, protected against experimental autoimmune encephalomyelitis. Our data suggest a model in which two distinct T_{reg} cell progenitor subsets both contribute to generate a broad T_{reg} cell repertoire able to protect against immune responses to self-antigen, limit immune responses to commensal organisms and resolve immune responses to foreign pathogens.

Results

CD25$^+$ and Foxp3^{lo} T_{reg}P cells differentiate into T_{reg} cells

To determine if CD25$^+$ and Foxp3^{lo} T_{reg}P are both bona-fide thymic T_{reg} progenitors we compared their ability to convert into mature T_{reg} cells in response to low doses of IL-2 for 3 days *in vitro*. Sorted CD25$^+$ T_{reg}P and Foxp3^{lo} T_{reg}P responded to very low amounts of IL-2 (0.2–1.0 U/mL) by converting to mature CD25$^+$Foxp3$^+$ T_{reg} cells (Supplementary Fig. 1a) indicating that although they lack CD25 expression, Foxp3^{lo} T_{reg}P, which express the low affinity IL-2R, consisting of the IL-2Rβ and IL-2Rγ chains, were responsive to IL-2. Mature CD25$^+$Foxp3$^+$ T_{reg} cells exhibited even greater sensitivity to IL-2, as they maintained their phenotype and viability at concentrations of IL-2 (0.04 U/mL) to which CD25$^+$ T_{reg}P and Foxp3^{lo} T_{reg}P cells did not respond (Supplementary Fig. 1a). To confirm these findings *in vivo*, we used ultrasound-guided intrathymic injection to co-transfer sorted congenically distinct (CD90.2$^+$CD45.2$^+$ or CD90.1$^+$CD45.2$^+$) CD25$^+$ or Foxp3^{lo} T_{reg}P cells into the thymi of CD45.1$^+$ mice (Fig. 1b, Supplementary Fig. 1b). Six days post-injection, total congenically labelled cells, derived from CD25$^+$ or Foxp3^{lo} T_{reg}P, were recovered from the host thymi with similar efficiency (data not shown). CD25$^+$ T_{reg}P and Foxp3^{lo} T_{reg}P cells converted into mature CD25$^+$Foxp3$^+$ T_{reg} cells with approximately the same frequency, although CD25$^+$ T_{reg}P did so slightly better (~45±16.9% to 37±23.5%, respectively; Fig. 1b). Thus, both CD25$^+$ T_{reg}P and Foxp3^{lo} T_{reg}P contributed to the generation of mature T_{reg} cells with high efficiency in vitro and in vivo.

CD25$^+$ T_{reg}P and Foxp3^{lo} T_{reg}P cells have distinct TCR repertoires

To address whether the CD25$^+$ T_{reg}P and Foxp3^{lo} T_{reg}P cells represent distinct subsets of cells with different TCR repertoires, or whether the T_{reg} cell developmental pathway chosen only reflects the stochastic expression of CD25 or Foxp3, we used mice expressing a fixed TCliβ *TCRb* transgene on a *TCRa*$^{+/-}$ heterozygous background expressing a Foxp3-RFP reporter [7, 8, 9]. Using these mice we carried out high throughput sequencing of the TCR *Trav14* genes in conventional CD25$^-$Foxp3$^-$ thymocytes, CD25$^+$ T_{reg}P, Foxp3^{lo} T_{reg}P and mature CD25$^+$Foxp3$^+$ T_{reg} cells. Consistent with previously published results [7, 10, 11], we found little overlap between the *Trav14* repertoire of conventional CD25$^-$Foxp3$^-$

thymocytes and mature thymic CD25$^+$Foxp3$^+$ T_{reg} cells (Fig. 2a). As reported [1], we found substantial overlap between the Trav14 repertoire of CD25$^+$ T_{reg}P cells and mature CD25$^+$Foxp3$^+$ T_{reg} cells (Fig. 2a,b, Table 1). Importantly, the TCR repertoire of the Foxp3^{lo} T_{reg}P also overlapped substantially with that of mature CD25$^+$Foxp3$^+$ T_{reg} cells (Fig. 2a). However, the TCR repertoires of the CD25$^+$ T_{reg}P and Foxp3^{lo} T_{reg}P cell populations showed very little overlap, despite their significant individual overlap with the repertoire of mature T_{reg} cells (Fig. 2a,b). To narrow our analysis to TCRs that are known to be represented in the mature T_{reg} cell pool, we reanalyzed our TCR repertoire data but this time excluding all the TCRs not detected in the thymic mature T_{reg} cell pool. The ratios of Morisita-Horn indices (T_{reg}P to T_{reg}P versus T_{reg}P to T_{reg} cell) calculated using TCRs detected only in mature CD25$^+$Foxp3$^+$ T_{reg} cells in the thymus were not significantly different than the ratios obtained when using all TCRs(Supplementary Table 1). Thus, CD25$^+$ T_{reg}P and Foxp3^{lo} T_{reg}P cells had distinct TCR repertoires and contributed unique TCR clones to the mature T_{reg} cell repertoire.

CD25$^+$ T_{reg}P and Foxp3^{lo} T_{reg}P cells have distinct affinity for self-antigen

Next we examined the types of antigens that CD25$^+$ T_{reg}P and Foxp3^{lo} T_{reg}P interacted with. The relative abundance of either T_{reg}P cell subset was similar in germ-free mice compared to specific pathogen-free mice (Supplementary Fig. 2a,b) or in C57Bl/6 mice co-housed with pet store mice, which have a normalized microbial experience [12], compared to specific pathogen-free mice (Supplementary Fig. 2c), suggesting that interactions with self antigens were the major driver of T_{reg} cell selection in the thymus. We used expression of the transcription factor Nur77, whose abundance is directly proportional to TCR signal strength, to assess the strength of the interaction of CD25$^+$ T_{reg}P and Foxp3^{lo} T_{reg}P cells with self-antigens in the thymus. In Nur77-GFP mice, in which GFP expression correlates with the strength of TCR stimulation [13, 14], mature CD25$^+$Foxp3$^+$ T_{reg} cells have higher expression of Nur77-GFP than conventional CD4$^+$Foxp3$^-$ T cells [3, 13, 14], corresponding with the higher degree of self-reactivity attributed to T_{reg} cells [7]. In this system, expression of Nur77-GFP in CD25$^+$ T_{reg}P cells was significantly higher compared to that recorded in mature T_{reg} cells (Fig. 2c,d), while the expression of Nur77-GFP in Foxp3^{lo} T_{reg}P cells was significantly lower than that of CD25$^+$ T_{reg}P cells (Fig. 2c,d). These findings indicate that CD25$^+$ T_{reg}P and Foxp3^{lo} T_{reg}P cells have distinct affinities for self-antigens in the thymus.

We next assessed the transcriptomic differences between the T_{reg}P subsets using single-cell RNA-Seq. CD25$^+$ T_{reg}P cells, Foxp3^{lo} T_{reg}P cells and mature, CD25$^+$Foxp3$^+$ T_{reg} cells sorted from thymi of *Foxp3*-GFP mice, in which an IRES-GFP construct was knocked into the3' UTR of the *Foxp3* gene, and were used to create individual single cell RNA-Seq libraries that were subjected to high-throughput sequencing. The transcriptomic data from these individual libraries was then combined for joint analysis. Individual cells were color-coded based on sort origin and a combined dimensional reduction with graph-based clustering approach followed by a shared nearest-neighbor modularity optimization-based clustering algorithm (Seurat R package) was applied to this combined data set to identify cell groups with distinct gene expression. This analysis generated clusters of cells that closely confirmed the original sorted populations (Fig. 2e), based on expression of *Il2ra* and *Foxp3* (Supplementary Fig. 3a). The analysis also identified a small subset of contaminating

thymocytes that expressed *Rag1*, *Cd8b1* and *Dntt* and therefore likely represent $CD4^+CD8^+$ double positive thymocytes (Fig. 2f). Heat maps based on the top ten most differentially expressed genes for each cell subset discriminated all four cell clusters (Fig. 2f). Analysis of differentially expressed genes indicated that there were ~180 reproducibly differentially expressed genes between $CD25^+$ and $Foxp3^{lo}$ $T_{reg}P$ cell subsets (Fig. 2f and Supplementary Table 2). Similar results were obtained in an independent single-cell RNA-Seq study with individually sorted $CD25^+$ $T_{reg}P$ cell, $Foxp3^{lo}$ $T_{reg}P$ cell and mature T_{reg} cell libraries (Supplementary Fig. 3b) or when $CD25^+$ $T_{reg}P$, $Foxp3^{lo}$ $T_{reg}P$ cells and mature T_{reg} cell subsets were combined into one library (data not shown). $CD25^+$ $T_{reg}P$ were enriched in pro-apoptotic genes and genes involved in negative selection (*Nr4a1* and *Bcl2l11*) (Supplementary Fig. 3c, Supplementary Table 2), consistent with stronger TCR signaling in this subset. $Foxp3^{lo}$ $T_{reg}P$ had increased expression of *Ms4a4b* and *Ms4a6b* (Fig. 2f), which encode MS4A4B and MS4A6B, which bind to GITR and enhance signaling via TCR and GITR [15] and may facilitate differentiation of lower affinity $CD4^+$ thymocytes into $Foxp3^{lo}$ $T_{reg}P$ and enhance sensitivity of $Foxp3^{lo}$ $T_{reg}P$ to IL-2 [3]. Thus, $CD25^+$ $T_{reg}P$ cells and $Foxp3^{lo}$ $T_{reg}P$ cells had distinct interactions with self-antigens presented in the thymus and unique transcriptomes indicative of distinct modes of selection and differentiation.

$CD25^+$ $T_{reg}P$ and $Foxp3^{lo}$ $T_{reg}P$ cells are at distinct developmental stages

The cell surface markers CD24 and Qa2, or CD69 and MHCI, can be used as surrogates to analyze thymocyte age [16]. We found that $CD25^+$ $T_{reg}P$ cells were largely $CD24^{hi}Qa2^{lo}$ (87%) and $CD69^{hi}$ $MHC1^+$, and thus representative of immature $CD4^+$ thymocytes. In contrast, only 38% of $Foxp3^{lo}$ $T_{reg}P$ cells were found in the $CD24^{hi}Qa2^{lo}$ gate with the remainder being $CD24^{lo}Qa2^{hi}$, indicative of a more mature stage of thymocyte development (Supplementary Fig. 4a,b). To examine this issue more precisely, we used *Rag2*-GFP transgenic mice, in which GFP expression is controlled by the *Rag2* gene regulatory elements, to determine the kinetics of differentiation for $CD25^+$ $T_{reg}P$ and $Foxp3^{lo}$ $T_{reg}P$ cells. The *Rag2-GFP* transgene turns off after positive selection in $CD4^+CD8^+$ thymocytes, after which the GFP protein decays with a relatively slow half-life, allowing GFP^+ recent thymic emigrants to be distinguished from older GFP^- T cells in peripheral blood and lymphoid organs [17]. To determine whether within the GFP^+ thymocyte fraction a gradient in GFP expression could distinguish thymocytes at different stages of development, we gated on $CD4^+$RAG2-GFP^+ thymocytes and examined CD25 and Foxp3 expression in different bins determined by expression of RAG2-GFP. RAG2-$GFP^{brightest}$ cells (bin 1) were all $CD25^-Foxp3^-$ CD4SP thymocytes (Fig. 3a). $CD25^+$ $T_{reg}P$, but no $Foxp3^{lo}$ $T_{reg}P$ cells or mature $CD25^+Foxp3^+$ T_{reg} cells were detected in bin 2, while $Foxp3^{lo}$ $T_{reg}P$ and mature $CD25^+Foxp3^+$ T_{reg} cells appeared in bin 3. $CD25^+$ $T_{reg}P$, $Foxp3^{lo}$ $T_{reg}P$ and mature $CD25^+Foxp3^+$ T_{reg} cells were all detected in bins 4–6, while $CD25^+$ $T_{reg}P$ cells were no longer detected in bin 7, as these cells differentiate, die or leave the thymus (Fig. 3a and Supplementary Video 1). Bin 8 contained GFP^- cells (Fig. 3a), representing fully mature recirculating T cells. This analysis indicated that the $CD25^+$ $T_{reg}P$ cells differentiated rapidly, while $Foxp3^{lo}$ $T_{reg}P$ cells took longer to develop.

About half of $CD25^+Foxp3^+$ T_{reg} cells in the thymus represent mature recirculating cells [18, 19]. Because 18% of $Foxp3^{lo}$ $T_{reg}P$ cells consisted of recirculating Rag2-GFP^- T cells

(Supplementary Fig. 5), we looked for cell surface markers that could distinguish newly developed RAG2-GFP$^+$ thymocytes from recirculating RAG2-GFP$^-$ T cells. Over 99% of CD73$^-$ cells were RAG2-GFP$^+$, while >85% of CD73$^+$ cells were RAG2-GFP$^-$ (Fig. 3b), suggesting expression of CD73 could distinguish between developing thymocytes and recirculating mature T cells in the thymus in the absence of the *Rag2-GFP* transgenic reporter. To assess whether Foxp3^{lo} T_{reg}P cells, which arose with slower kinetics and exhibited reduced TCR signal strength, were more dependent on adhesion molecules like LFA-1, which help prolong T cell-APC contacts and enhance TCR signaling [20], we examined T_{reg} cell development in *Itgal*$^{-/-}$ mice, which are LFA-1 deficient. CD73$^-$ Foxp3^{lo} T_{reg}P, but not CD73$^-$ CD25$^+$ T_{reg}P cells were decreased in *Itgal*$^{-/-}$ thymi compared to wild-type thymi (Fig. 3c). Thus, development of Foxp3^{lo} T_{reg}P cells was more dependent on stable T cell-APC interactions or LFA-1-dependent co-stimulation compared to CD25$^+$ T_{reg}P cells.

Based on Foxp3 overexpression studies, Foxp3^{lo} T_{reg}P cells were proposed to be very susceptible to apoptosis [6]. Because our single cell RNA-Seq, based on *Bcl2l11* and *Nr4a1* expression, suggested that CD25$^+$ T_{reg}P cells might be more apoptotic than Foxp3^{lo} T_{reg}P cells (Supplementary Fig. 3c, Supplementary Table 2) we used annexin V staining to identify apoptotic cells in the thymus. Annexin V$^+$ cells were detected in both T_{reg}P cell subsets, although there were substantially more annexin V$^+$ cells in the CD73$^-$ CD25$^+$ T_{reg}P (12%) than in the CD73$^-$ Foxp3^{lo} T_{reg}P cells (3.3%; Fig. 3d). We also stained thymocytes for cleaved caspase-3 (casp-3). CD25$^+$ T_{reg}P were enriched four-fold for casp-3$^+$ cells compared to Foxp3^{lo} T_{reg}P cells (Fig. 3e). Thus, CD25$^+$ T_{reg}P cells interacted most strongly with self-antigen in the thymus and contained a higher fraction of apoptotic cells, suggesting they were undergoing negative selection.

We next examined where Foxp3^{lo} TregP were located in the thymus. Histocytometry [21] experiments in C57Bl/6 mice thymi indicated that mature CD25$^+$Foxp3$^+$ T_{reg} cells were largely restricted to the thymic medulla (Fig.4a,b), consistent with agonist-driven T_{reg} selection occurring in the thymic medulla. In contrast, Foxp3^{lo} T_{reg}P cells were found both in the thymic medulla and some (20%) in the thymic cortex (Fig. 4 a,b), suggesting that at least some Foxp3^{lo} T_{reg}P cells were selected on cortical antigens. Thus, CD25$^+$ and Foxp3^{lo} T_{reg}P subsets differentiate with distinct kinetics and exhibit different rates of apoptosis; moreover, a fraction of the Foxp3^{lo} T_{reg}P subset share features with conventional (i.e., non-Treg) T cells undergoing positive selection, which also occurs in the thymic cortex.

NF-kB is critical for the development of Foxp3^{lo} T_{reg}P cells

We next assessed the effect of co-stimulation and downstream signaling pathways on the development of CD25$^+$ T_{reg}P and Foxp3^{lo} T_{reg}P. *Cd28*$^{-/-}$ thymi exhibited a 1.7-fold decrease in abundance of CD25$^+$ T_{reg}P, and a 6.7-fold decrease in abundance of Foxp3^{lo} T_{reg}P compared to thymi from wild-type mice (Fig. 5a). Similar results were found in CD28-AYAA mice, which express a mutant CD28 lacking the PYAP motif that links CD28 to activation of the transcription factor NF-κB (data not shown), but not in CD28-Y170F mice, which express a mutant CD28 lacking Y170, which links CD28 to signaling through PI3K (data not shown). Conversely, IKK-CA mice, which express a constitutively active

from of IKK that leads to constitutive NF-κB activation, had a selective increase in Foxp3^{lo} T_{reg}P cells (data not shown). A caveat of the analysis in CD28-AYAA, CD28-Y170F and IKK-CA mice is the lack of CD73 staining to exclude recirculating mature effector T cells and T_{reg} cells from the CD25^{+}Foxp3^{-} T_{reg}P and CD25^{-}FOXP3^{lo} T_{reg}P gates, respectively. Finally, we examined the effect of the downstream transcription factor NF-κB1 on T_{reg} cell development. *Nfkb1*$^{-/-}$ mice had a 3.6 fold reduction in the abundance of CD73^{-}Foxp3^{lo} T_{reg}P cells compared to thymi from wild-type mice, while CD73^{-}CD25^{+} T_{reg}P cell abundance was unaffected (Fig. 5b). These results suggest that co-stimulation, and especially activation of NF-κB1, were selectively required for the formation of Foxp3^{lo} T_{reg}P.

CD25^{+} T_{reg}P and Foxp3^{lo} T_{reg}P development is regulated by distinct enhancers

To examine whether Foxp3 was required for the development of T_{reg} cells from both CD25^{+} T_{reg}P and Foxp3^{lo} T_{reg}P we used *Foxp3-GFP*^{KIN} mice, in which a GFP reporter construct is knocked-into the *Foxp3* locus and generates a GFP-Foxp3 fusion protein [22]. These mice express normal amounts of GFP-Foxp3 protein, but have been described as functional Foxp3 hypomorphs [23, 24]. Following gating on CD4^{+}CD73^{-} thymocytes, we found that *Foxp3-GFP*^{KIN} mice had a significant reduction in the frequency Foxp3^{lo} T_{reg}P compared to thymi from wild-type mice, while the abundance CD25^{+} T_{reg}P was unaffected (Fig. 5c). To examine this in more detail we analyzed *Foxp3-GFP*^{KIN} mice lacking the *Foxp3* regulatory element *Cns3* (called *Cns3*$^{-/-}$ mice hereafter). *Cns3*$^{-/-}$ mice, which are known to have a ~40% reduction in the frequency of T_{reg} cells in the thymus [25], have selective defects in immune tolerance and a T_{reg} cell bias towards higher self-reactivity [26]. *Cns3*$^{-/-}$ mice lacked Foxp3^{lo} T_{reg}P cells (Fig. 5c). Consistent with previous reports [25], mature CD25^{+}Foxp3^{+} T_{reg} cells were also substantially reduced in *Cns3*$^{-/-}$ mice compared to wild-type mice, and the defect was about twice as large (~80% reduction) when gating on CD73^{-} cells to eliminate mature recirculating T_{reg} cells (Fig. 5c). Importantly, mature CD25^{+}Foxp3^{+} CD73^{+} T_{reg} cells in *Cns3*$^{-/-}$ and wild-type mice expressed comparable amounts of Foxp3 (Supplementary Fig. 6a), indicating that *Cns3* was not required for Foxp3 expression. CD25^{+} T_{reg}P cells isolated from wild-type, *Foxp3-GFP*^{KIN} or *Cns3*$^{-/-}$ mice cultured in vitro upregulated Foxp3 and differentiated into mature CD25^{+}Foxp3^{+} T_{reg} cells with comparable efficiency when stimulated with IL-2 (Fig. 5d), suggesting *Cns3* was not required for the expression of *Foxp3* in mature T_{reg} cells. These results indicated that the development of T_{reg} cells from Foxp3^{lo} T_{reg}P was blocked in the absence of *Cns3* and mature T_{reg} cells developed only from CD25^{+} T_{reg}P cells in *Cns3*$^{-/-}$ mice.

A non-coding SNP that contributes to an increased risk for autoimmunity in humans was previously described in the *Il2ra* locus [27, 28, 29], specifically in enhancer CaRE4, which is required for rapid induction of *Il2ra* following TCR activation [30]. Next, we examined the role of this autoimmunity-associated *Il2ra* enhancer in T_{reg} cell development. Deletion of the CaRE4 *Il2ra* enhancer in the NOD mice background led to a significant reduction in the percentages of thymic CD25^{+} T_{reg}P cells and mature T_{reg} cells compared to wild-type NOD mice (Fig. 5e). In contrast, the percentage of Foxp3^{lo} T_{reg}P cells was slightly increased, perhaps as a compensatory mechanism. This decrease in CD25^{+} T_{reg}P cells was not due to a lack of CD25 expression in general, as the expression of CD25 on mature T_{reg} cells, or on

the remaining CD25$^+$ T_{reg}P, was not reduced compared to wild-type controls (Supplementary Fig. 6b and data not shown). Collectively these data suggest that the development of T_{reg} cells from CD25$^+$ T_{reg}P and Foxp3^{lo} T_{reg}P cells was controlled by distinct regulatory circuits.

Inhibition of negative selection pathways expand CD25$^+$ T_{reg}P cells

To further probe if CD25$^+$ T_{reg}P cells were undergoing negative selection, we examined the development of T_{reg} cells in *Itk*$^{-/-}$ mice, as mice lacking the tyrosine kinase ITK have defects in negative selection [31]. *Itk*$^{-/-}$ thymi had higher frequencies of mature thymic CD25$^+$Foxp3$^+$ T_{reg} cells [32], as well as CD25$^+$ T_{reg}P and Foxp3^{lo} T_{reg}P cells (Fig. 6a). The adaptor protein ADAP, which is downstream of ITK, is also required for efficient negative selection[33]. Thymi from *Adap*$^{-/-}$ mice showed an increase in the abundance CD25$^+$ T_{reg}P, but no change in Foxp3^{lo} T_{reg}P cells compared to wild-type (Fig. 6b). The frequency of mature CD25$^+$Foxp3$^+$ T_{reg} cells in the thymus was also significantly increased in *Adap*$^{-/-}$ mice compared to wild-type (Fig. 6b). Thus, *Adap*$^{-/-}$ mice have a selective increase in CD25$^+$ T_{reg}P cells compared to wild-type mice. A potential explanation for the discrepancy between *Itk*$^{-/-}$ and *Adap*$^{-/-}$ mice is that ITK deficiency is known to induce increased production of IL-4 in iNKT cells in the thymus [34, 35], while ADAP deficiency does not. To examine if the different phenotypes in terms of T_{reg} cell development in *Adap*$^{-/-}$ and *Itk*$^{-/-}$ mice were linked to IL-4 production we examined T_{reg} cell development in *Itk*$^{-/-}$ and *Itk*$^{-/-}$ *x Il4ra*$^{-/-}$ mice. Compared to *Itk*$^{-/-}$ mice, the increase in abundance of Foxp3^{lo} T_{reg}P cells was lost in the thymi of *Itk*$^{-/-}$ *x Il4ra*$^{-/-}$ mice (Fig. 6a,c), suggesting that the increase in Foxp3^{lo} T_{reg}P cells in *Itk*$^{-/-}$ mice was due to the increased amounts of IL-4 present in the thymi of these mice. Thus CD25$^+$ TregP cells are selectively pruned by the ITK-ADAP pathway required for negative selection.

CD25$^+$ T_{reg}P and Foxp3^{lo} T_{reg}P cells have distinct cytokine responsiveness

IL-2, and to a lesser degree IL-15, are the predominant cytokines that drive the STAT5-dependent differentiation of CD25$^+$ T_{reg}P cells into mature T_{reg} cells [1, 2, 4, 36, 37]. Because the ability of Foxp3^{lo} T_{reg}P cells to differentiate into mature T_{reg} cells in response to IL-4 has not been evaluated, we asked if IL-4 could affect the differentiation of CD25$^+$ T_{reg}P or Foxp3^{lo} T_{reg}P cell subsets into mature T_{reg} cells. As reported previously [1, 37], IL-4 did not cause robust conversion of thymically derived CD25$^+$ T_{reg}P cells into mature T_{reg} cells, but supported substantial conversion of thymically-derived Foxp3^{lo} T_{reg}P into mature CD25$^+$Foxp3$^+$ T_{reg} cells in an *in vitro* assay (Fig. 7a). Foxp3^{lo} T_{reg}P had slightly higher expression of the IL-4 receptor (IL-4Ra) compared to CD25$^+$ T_{reg}P (Fig. 7b), which we considered unlikely to account for the difference in the differentiation of CD25$^+$ T_{reg}P and Foxp3^{lo} T_{reg}P cells in response to IL-4. In addition, although IL-4 converted Foxp3^{lo} T_{reg}P cells into mature T_{reg} cells, these cells expressed less CD25 and Foxp3 than those stimulated with IL-2 alone (Supplementary Fig. 7a–d).

What cells drive production of IL-4 in the thymus remains unclear. In humans, the Hassall's corpuscles, a distinct anatomical feature of the thymus containing cells that resemble Tuft cells, are important for T_{reg} cell development [38]. Tuft cells were also reported in the murine thymi [39, 40] and are major producers of IL-25, which induces IL-4 production in other cell

types [41]. To test whether thymic tuft cells influenced $T_{reg}P$ cell differentiation, we examined T_{reg} cell development in *Pou2f3*$^{-/-}$ mice, which lack the transcription factor POU2F3, which is required for the development of tuft cells. We observed an ~30% decrease in frequency of Foxp3^{lo} $T_{reg}P$, but not CD25^{+} $T_{reg}P$ cell development in *Pou2f3*$^{-/-}$ thymi compared to wild-type (Fig. 7c). To determine if iNKT cells, the canonical producers of IL-4 in the thymus, selectively affected the development of Foxp3^{lo} $T_{reg}P$ cells we examined the frequency of $T_{reg}P$ in *Cd1d*$^{-/-}$ mice, which lack NKT cells. There was an ~20% reduction in the abundance of Foxp3^{lo} $T_{reg}P$ cells in the *Cd1d*$^{-/-}$ thymi compared to wild-type Balb/c controls (Fig. 7d). This effect was only observed in Balb/c mice, which produce abundant NKT-derived IL-4, and not in C57Bl/6 mice, in which NKT cells make very little IL-4 (data not shown). Thus, CD25^{+} $T_{reg}P$ and Foxp3^{lo} $T_{reg}P$ cells development have distinct dependence on thymic tuft cells, and this is likely partially mediated via tuft cell induction of IL-4 production in iNKT cells.

CD25^{+} and Foxp3^{lo} TRP exhibit distinct functions

Next we tested whether the mature T_{reg} cells derived from CD25^{+} $T_{reg}P$ or Foxp3^{lo} $T_{reg}P$ cells had different abilities to prevent distinct types of autoimmune diseases, driven by different auto-antigens. To test whether mature T_{reg} cells generated from CD25^{+} $T_{reg}P$ cells differed in their ability to suppress autoimmunity in the central nervous system when compared to Foxp3^{lo} $T_{reg}P$-generated T_{reg} cells, we isolated thymic CD25^{+} $T_{reg}P$ or Foxp3^{lo} $T_{reg}P$ cells, transferred them separately into individual C57Bl/6 host mice 1 day before immunization with $MOG_{35–55}$ peptide and monitored the development of EAE symptoms. Transfer of mature T_{reg} cells is known to prevent or ameliorate symptoms in this EAE model [42]. Mice receiving Foxp3^{lo} $T_{reg}P$ showed similar disease scores throughout the study as mice without $T_{reg}P$ transfer (Fig. 8a). In contrast, disease progression and severity in mice that received CD25^{+} $T_{reg}P$ were significantly blunted from day 14 through 18 after disease induction compared to mice receiving no $T_{reg}P$ or Foxp3^{lo} $T_{reg}P$ cells (Fig. 8a,b). The number of congenically-marked donor Foxp3^{+} T_{reg} cells observed following transfer of CD25^{+} or Foxp3^{lo} $T_{reg}P$ cells was similar in the spleen at the endpoint of the experiment, 20 days after $T_{reg}P$ transfer (Fig. 8c), suggesting the conversion of CD25^{+} $T_{reg}P$ and Foxp3^{lo} $T_{reg}P$ into mature T_{reg} cells was similar. However, transferred Foxp3^{lo} $T_{reg}P$ cells prevented weight loss in a T cell transfer model of colitis (Supplementary Fig. 8), demonstrating the suppressor activity of the Foxp3^{lo} $T_{reg}P$-derived T_{reg} cells was normal. Finally, we used MOG:I-A^{b} tetramers in combination with magnetic bead enrichment approaches to identify MOG:I-A^{b}-specific T_{reg} cells and $T_{reg}P$ in the thymus of wild-type mice. We found MOG:I-A^{b}-specific T cells in the CD25^{+} $T_{reg}P$ and mature T_{reg} cell subsets, but only observed one MOG:I-A^{b}-specific T cell in the Foxp3^{lo} $T_{reg}P$ in 15 mice examined (Fig. 8d,e), suggesting MOG:I-A^{b}-specific T_{reg} cells were almost always generated from the CD25^{+} $T_{reg}P$ and were specifically required for protection against EAE.

Discussion

Here we found that both CD25^{+} $T_{reg}P$ and Foxp3^{lo} $T_{reg}P$ contributed to mature T_{reg} development in the thymus, and that in our hands they did so relatively equivalently. However, these two distinct TregP cell subsets differed in many important ways. They

utilized different signaling pathways and enhancers for their differentiation, were affected in distinct ways by different stromal cells and cytokines and expressed distinct TCR repertoires and RNA transcriptomes. Most importantly, T_{reg} cells derived from $CD25^{+}T_{reg}P$ versus $Foxp3^{lo}$ $T_{reg}P$ subsets had distinct roles in protecting against autoimmunity. Thus, there are at least two different developmental pathways in the thymus that contribute substantially to the generation of the mature T_{reg} cell repertoire.

Several pieces of evidence support the notion that mature T_{reg} cells derived from both $CD25^{+}$ $T_{reg}P$ and $Foxp3^{lo}$ $T_{reg}P$ cells are required for full maintenance of immune tolerance. Both the *Foxp3-GFP*^{KIN} hypomorph and *Cns3*$^{-/-}$ mice had defects in generating $Foxp3^{lo}$ $T_{reg}P$ and specific defects in immune tolerance. The *Foxp3-GFP*^{KIN} mice have a relatively mild defect in immune tolerance that is only revealed on distinct genetic backgrounds[23, 24]. In contrast, *Cns3*$^{-/-}$ mice have unique defects in immune tolerance, such as greater inflammation in the lung than wild-type mice[26]. In addition, *Cns3*$^{-/-}$ mice have increased titers of specific autoantibodies [26]. Because *Cns3*$^{-/-}$ mice selectively lacked $Foxp3^{lo}$ but not $CD25^{+}$ $T_{reg}P$, this suggests a unique role for $Foxp3^{lo}$ $T_{reg}P$-derived mature T_{reg} cells in preventing autoimmunity.

Additional studies suggest a unique role for $CD25^{+}$ $T_{reg}P$ in promoting immune tolerance. The *CaRE4* enhancer in the *Il2ra* locus harbors an autoimmunity risk variant that promotes susceptibility to inflammatory bowel disease, but protection against diabetes [27, 28, 29]. Deletion of this enhancer resulted in a selective decrease in $CD25^{+}$ $T_{reg}P$, suggesting that $CD25^{+}$ $T_{reg}P$-derived T_{reg} cells could have an important role in protecting against inflammatory bowel disease. Likewise, *Cns3*$^{-/-}$ mice exhibit increased protection against EAE [26]. Because T_{reg} cells in *Cns3*$^{-/-}$ mice are almost exclusively derived from $CD25^{+}$ $T_{reg}P$, this suggests $CD25^{+}$ $T_{reg}P$ -derived T_{reg} cells protect against EAE. We directly confirmed this idea by showing that $CD25^{+}$ $T_{reg}P$-derived T_{reg} cells provided robust protection from EAE while $Foxp3^{lo}$ $T_{reg}P$-derived T_{reg} cells did not. Thus, modulating the frequency of $CD25^{+}$ $T_{reg}P$ results in differential protection against autoimmunity. This observation has important translational implications, as it indicates that T_{reg} cells with select TCRs can be identified that have uniquely potent efficacy versus specific types of autoimmune disease.

The presence of more than one developmental pathway leading to mature T_{reg} cells raises the question of why such a system has evolved. T_{reg} cells are required to prevent responses to self-antigens and commensal antigens, as well as dampen anti-pathogen immune responses once these agents have been cleared. Establishing such a diverse repertoire requires the generation of T_{reg} cells able to recognize high-affinity self-antigens. Such a population could be generated via a process of agonist selection in the thymus. However, agonist selection is unlikely to generate the broad repertoire of T_{reg} cells needed to prevent immune responses to commensal organisms or to limit responses to foreign pathogens. In many ways this resembles the problem faced by conventional thymocytes, which must generate a repertoire able to recognize a vast array of antigens that they never see in the thymus. Thus, establishing a broader non-self-focused repertoire for T_{reg} cells may require a process that resembles positive selection for conventional thymocytes. We show that T_{reg} cells developed through two distinct developmental programs that exhibit such

characteristics. $CD25^+$ $T_{reg}P$ developed through a process of agonist selection that shared many similarities with the underlying process of negative selection and would result in mature T_{reg} cells focused on TCRs with high-affinity for thymic self-antigens. $Foxp3^{lo}$ $T_{reg}P$ developed through a mechanism that could be akin to positive selection of T_{reg} cells, resulting in a broader repertoire able to react with both self- and non-self antigens. As such, thymic T_{reg} cells derived from $Foxp3^{lo}$ $T_{reg}P$ could complement the function of induced peripheral T_{reg} cells. Our model also suggests that the *Cns3* regulatory element evolved to promote the development of mature T_{reg} cells through the $Foxp3^{lo}$ $T_{reg}P$ pathway. Finally, the genetic variability that altered the relative balance of these two developmental pathways also altered the T_{reg} cell repertoire and correlated with susceptibility to distinct forms of autoimmunity. Given the differences in signaling pathways and cytokines that controlled these two developmental pathways, specific targeting of each T_{reg} cell population might help patients with various autoimmune defects.

Online Methods

Mice.

Mice were housed in specific pathogen–free facilities at the University of Minnesota, Cornell University, Salk Institute or University of California San Francisco, and experiments were in accordance with protocols approved by the Institutional Animal Care and Use Committees of these respective institutions. Exceptions are germ-free mice housed in germ-free facilities at the University of Chicago and mice with a normalized microbial experience which were housed in the University of Minnesota's mouse vivarium. Pet store mice were purchased from various pet stores in the greater Minneapolis-St. Paul metropolitan area. Information about the age of the pet store mice was not available from the vendor. Co-housing of SPF mice with sex-matched pet store partner was performed as described[12] within the University of Minnesota BSL-3 facility. Conversion efficiency was confirmed by assessing the conversion of naïve $CD8^+$ T cells into $CD8^+$ memory T cells; effective conversion correlated with ~30–60% $CD8^+CD44^{hi}$ T cells. All relevant ethical guidelines have been followed. *Foxp3-GFP* mice (006772), *Foxp3-RFP* mice (008374) were from the Jackson Laboratory. $CD45.1^+$ (B6.SJL) mice were from the US National Cancer Institute. *Nur77-GFP* BAC reporter mice, *Rag2-GFP* reporter mice, $Cns3^{-/-}$ and $Foxp3\text{-}GFP^{KI}$, $CD28^{-/-}$, $Nfkb1^{-/-}$, $Itk^{-/-}$, $Itk^{-/-}$ *x* $Il4Ra^{-/-}$, $Adap^{-/-}$, *Il2ra EDEL*, $Itgal^{-/-}$, $Rag2^{-/-}$, $Cd1d^{-/-}$ and *Tcliβ x* $TCR\alpha^{+/-}$ have been described previously [7, 14, 17, 22, 25, 30, 35, 43, 44, 45, 46, 47, 48]. Mice were generally six to eight weeks old but ranged from four to sixteen weeks old. Mice were randomly selected for experiments, in age-matched cohorts. The investigators were not 'blinded' to genotype during data acquisition.

Tissue preparation and cell isolation.

For analysis of thymocyte and Treg development thymi were mechanically dissociated into 1x PBS with 2% FBS and 2 mM EDTA, pH 7.4, using frosted glass slides. Cells suspensions were passed through 70 μm filters and washed prior to staining.

Flow cytometry and antibodies.

All flow cytometry analysis was conducted in the University of Minnesota Flow Cytometry Core Facility using BD LSR II and Fortessa cytometers (BD, San Jose, CA). For surface staining, cells were stained for 20 minutes with fluorochrome-conjugated antibodies prior to washing and analysis or intracellular staining. Intracellular detection of Foxp3, Cleaved Caspase-3 and GFP was performed as previously described [2] using the eBioscience Transcription Factor staining kit. When staining for GFP, *Rag2-GFP* thymi were fixed for 10 minutes at room temperature in 1.6% PFA prior to intracellular staining of GFP and Foxp3 using the eBioscience Transcription Factor staining kit. For apoptosis assays, thymi were harvested and mechanically dissociated into 1x PBS on ice. Following surface staining cells were washed into Annexin V binding buffer (eBioscience San Diego, CA) and stained with Annexin V. Specific antibodies used are listed below. For tetramer staining, single cell thymocyte suspensions were treated with Dasatinib (Axon Medchem) at 50nM in complete RPMI for 20 minutes at 37°C followed by dual (APC and PE conjugated) $MOG_{38–48}$ tetramer [49] staining at 10nM for an additional 45 minutes in complete RPMI (10% FBS, 1% glutamine, 1% penicillin-streptomycin, 1% NEAA, 10mM HEPES, 50uM BME) at 37°C. Tetramer stained cells were washed and incubated with anti-APC and anti-PE microbeads (Miltenyi Biotec) for 30 minutes on ice. Cells were washed and run over a LS column and unbound and bound fractions were collected, stained and analyzed as described above. A complete list of staining reagents is available as a supplemental reagent table.

Ultrasound guided intrathymic injection

Injections were performed largely as described previously [50]. Briefly, mice were anesthetized with 2–4% isofluorane in medical gas (21% oxygen, 79% nitrogen) in an acrylic chamber then transferred to the warmed ultrasound platform face up with the snout fastened in a facemask delivering 2–4% isofluorane and medical gas. Depilatory cream was used to remove hair from the mid-upper ventral thoracic region prior to applying ultrasound gel. Using the Vevo 2100 ultrasound, the MS550D probe was lowered parallel to the left or right side of the sternum. The ultrasound image generated was used to guide an insulin syringe (27G) into the thymus and visualize the injection of the 10–20uL cell suspension.

Immunofluorescence and histo-cytometry

Immunofluorescence analysis of thymi was described previously [51]. Thymi were washed, fixed with 4% paraformaldehyde (PFA) for 1 h and snap frozen. 5-μm sections were blocked with PBS containing 5% bovine serum albumin (BSA) and goat serum (Jackson Laboratory) before staining. The sections were then covered with Prolong anti-fade mounting medium (Life Technologies) and images were obtained 1 to 3 d later with a Leica DM6000B Epi-Fluorescent microscope.

Histo-cytometry analysis was performed as described previously [21].

TCR sequencing

CD4SP thymocytes were enriched by magnetic depletion using biotinylated anti-CD8/Ter119 antibodies followed by secondary labelling with streptavidin–conjugated microbeads (Miltenyi Biotec). Enriched cells are labelled with fluorchrome-conjugated anti-CD4, CD25

and streptavidin, while Foxp3 is marked with the RFP reporter, prior to sorting on the BD Aria sorter (BD Biosciences). TCR sequencing was performed as described previously [52]. Briefly, $CD4^+CD25^-Foxp3^-$, $CD4^+CD25^+Foxp3^-$, $CD4^+CD25^-Foxp3^{lo}$ and $CD4^+CD25^+Foxp3^+$ populations are sorted into lysis buffer (Buffer RLT+BME). cDNA was generated from these samples using the RNeasy kit (QIAGEN Valencia, CA). CDR3 Vα2 TCRs were sequenced using an Ion Torrent as previously described. TCRs representing >20% of the reads in the T_{reg} compartment, which influence distributions disproportionally, were excluded from analysis as described [53].

T_{reg} progenitor conversion assays.

T_{reg} progenitors were isolated as previously described [2]. Briefly, *Foxp3-GFP* thymi were dissected, dissociated, and pooled CD4SP cells were enriched by magnetically depleting with biotinylated anti-CD8 and Ter119 antibodies (eBioscience) followed by secondary labeling with streptavidin-conjugated microbeads (Miltenyi Biotec). Enriched CD4SP cells were stained with fluorchrome-conjugated anti-CD4, CD25, CD73 and streptavidin prior to sorting $CD4^+CD73^-CD25^+GFP^-$, $CD4^+CD73^-CD25^-GFP^+$, or $CD4^+CD73^-CD25^+GFP^+$ cells using a BD Facs Aria sorter (BD Biosciences). Purified T_{reg} cell progenitors or T_{reg} cells were incubated in complete RPMI and supplemented with human IL2 from R&D Systems (Minneapolis, MN) or mouse IL4 from Tonbo Biosciences (San Diego, CA). After 72 hours, cells were harvested, stained with anti-CD4, CD8 and CD25 antibodies and analyzed by flow cytometry for the percentage or number of cells that express CD25 and GFP after incubation.

Mapping and analysis of single cell sequencing

$CD4^+CD73^-CD25^+Foxp3^-$, $CD4^+CD73^-CD25^-Foxp3^{lo}$ and $CD4^+CD73^-CD25^+Foxp3^+$ cells were isolated from a single *Foxp3-GFP* thymus using a BD Facs Aria sorter. Cells were resuspended at 10^6 cells/mL in 50%FBS in 1xPBS before being counted and captured using the 10X Genomics (San Francisco, CA) Single Cell 3' Solution.

A custom genome was created by adding the sequence for the FoxP3-GFP construct [54] as a new chromosome to the Ensembl GRCm38 reference and gtf file (version 89). The gene annotation file (gtf) was then filtered further to contain only protein coding genes. The 10x Genomic Cellranger pipeline (version 2.2.0 https://support.10xgenomics.com/single-cell-gene-expression/software/overview/welcome) was used to align reads and generate counts for each sorted population (or library). Sorted populations were then combined using the depth normalization mode.

The Seurat R Package (version 1.4.0.12) was used to analyze the mapped single cell reads. The data was filtered to include cells that contained 100–2500 unique gene counts and expressed more than 5 genes. Global-scaling normalization was applied to the filtered data as described in the default settings in the Seurat package. The data was then scaled to regress out sequencing depth. Linear dimensional reduction (PCA) was performed on the most variable genes (2010 genes). Heatmap analysis of different PCs and an elbow plot were created to decide on proceeding with 9 PCs for cluster analysis using the Seurat function 'FindCluster'. To visualize the clusters, non-linear dimensional reduction (tSNE) was

performed using the 9 PCs. Clusters were assigned to a specific population by comparing cells labeled for the original sorted population and cellular markers. The R packages plot3D (version 1.1.1) and threejs (version 0.3.1) were used to create 3D visualization of the tSNE data. Differential expression ("bimod" McDavid et al., 2013) was calculated for each cluster against all other clusters to identify potential markers for each individual cluster. Differential expression was also calculated between individual clusters using the same method.

Experimental Autoimmune Encephalomyelitis Induction

EAE was induced in mice as described previously [55]. Briefly, on Day −1 sorted $T_{reg}P$ populations (4×10^5-5×10^5) were transferred i.v. into CD45.1 congenic mice. On Day 0 mice were immunized with 200ug of $MOG_{35–55}$ emulsified in CFA with 4mg/mL heat killed Tb. Immunization was performed with 2, 50uL s.c. injections of emulsion on left/right flank of the lower back. Mice were treated with 200ng Pertussis Toxin on day 0 and day 2 via i.p. injection in 1xPBS. Mice were monitored for disease progression and treated with s.c. normal saline or given wet food on the cage floor, as described previously [55].

Transfer colitis induction

Colitis was induced as previously described [56]. Briefly, 5×10^5 $CD4^+CD45RB^{hi}$ cells were transferred via i.v. or i.p. injection into *Rag*$^{-/-}$ recipient mice. Sorted $T_{reg}P$ were transferred via i.p. injection in a split dose (2.5×10^5 on days 1 and 7) or a single dose (5×10^5 on day 21). Mice were weighed weekly to monitor disease progress.

Statistical analysis

Statistical tests used to analyze data are included within the figure legends. Briefly, comparisons of 2 groups were done by either, paired *t*-test (paired, normal data), Wilcoxon matched-pairs test (paired, non-normal data), *t*-test (non-paired, normal data) or Mann-Whitney (non-paired, non-normal data); tests were always two-sided. Comparisons of 3 or more groups was done by one-way ANOVA (non-paired, normal data), Kruskal-Wallis (non-paired, non-normal data), or Friedman test (paired, non-normal data). P-values <0.05 were considered significant. Statistics were calculated using Prism (GraphPad Software, LaJolla, CA). All data, except those specifically mentioned in figure legends, are displayed as mean ± standard deviation.

Supplementary Material

Refer to Web version on PubMed Central for supplementary material.

Acknowledgements

We thank G. Hubbard, A. Rost, A. Meskic, D. Duerre and H. Wiesolek for technical assistance, T. Martin, N. Shah, J. Motl and P. Champoux for cell sorting and maintenance of the Flow Cytometry Core Facility at the University of Minnesota (5P01AI035296), S. Hamilton, M. Pierson and funding from the University of Minnesota academic health center for maintaining the NME mouse facility, P. Fink for providing initial *Rag2-GFP* thymi, B. Burbach and Y. Shimizu for *Adap*$^{-/-}$ mice, M. Jenkins and T. Dileepan for MOG:I-Ab tetramer, and C. Katerndahl and L. Heltemes-Harris for helpful commentary and for reviewing the manuscript. D.L.O. and S.A.M. were supported by an immunology training grant (2T32AI007313). S.A.M. was also supported by an individual predoctoral F30 fellowship from the NIH (F30DK096844). J.A.S. was supported by University of Minnesota Medical Foundation grant UMF0020624 and NIH grants 5U24AI118635 and R01AI106791. Y.Z. was supported by NIH grant

R01AI107027, U.B. and C.B.W. were supported by grants from the Children's Hospital of Wisconsin, C.B.W. was also supported by NIH grant R01AI085090–07A1, A.M. and M.S.A were supported by NIH grant DP3DK111914–01 and A.M. holds a Career Award for Medical Scientists from the Burroughs Wellcome Fund and is an investigator at the Chan Zuckerberg Biohub, M.A. was supported by NIH grant R01AI115716, M.S.A. was supported by NIH grant R37 AI097457, A.A. was supported by NIH grants AI108958, AI120701, AI126814, and AI129422 to A.A. and W.H., W.H. was supported by NIH grant AI29422 (to WH and AA) a Careers in Immunology Fellowship from the American Association of Immunologists, a Faculty Development Award, and a competitive research grant from Louisiana State University, and a pilot award from the LSU-Tulane Center for Experimental Infectious Diseases Research funded by NIH grant GM110760. M.A.F. was supported by NIH grants AI124512, AI113138, AI061165, CA154998, CA151845, and CA185062.

A.M. is a co-founder of Spotlight Therapeutics. A.M. has served as an advisor to Juno Therapeutics and is a member of the scientific advisory board at PACT Pharma. The Marson laboratory has received sponsored research support from Juno Therapeutics, Epinomics and Sanofi, and a gift from Gilead. AA has received sponsored research support from 3M. MAF has received sponsored research support from Merck.

References

1. Lio CW & Hsieh CS A two-step process for thymic regulatory T cell development. Immunity 28, 100–111 (2008). [PubMed: 18199417]
2. Burchill MA et al. Linked T cell receptor and cytokine signaling govern the development of the regulatory T cell repertoire. Immunity 28, 112–121 (2008). [PubMed: 18199418]
3. Mahmud SA et al. Costimulation via the tumor-necrosis factor receptor superfamily couples TCR signal strength to the thymic differentiation of regulatory T cells. Nature immunology 15, 473–481 (2014). [PubMed: 24633226]
4. Burchill MA, Yang J, Vogtenhuber C, Blazar BR & Farrar MA IL-2 receptor beta-dependent STAT5 activation is required for the development of Foxp3+ regulatory T cells. J Immunol 178, 280–290 (2007). [PubMed: 17182565]
5. Yao Z et al. Nonredundant roles for Stat5a/b in directly regulating Foxp3. Blood 109, 4368–4375 (2007). [PubMed: 17227828]
6. Tai X et al. Foxp3 transcription factor is proapoptotic and lethal to developing regulatory T cells unless counterbalanced by cytokine survival signals. Immunity 38, 1116–1128 (2013). [PubMed: 23746651]
7. Hsieh CS et al. Recognition of the peripheral self by naturally arising CD25+ CD4+ T cell receptors. Immunity 21, 267–277 (2004). [PubMed: 15308106]
8. Fenton RG, Marrack P, Kappler JW, Kanagawa O & Seidman JG Isotypic exclusion of gamma delta T cell receptors in transgenic mice bearing a rearranged beta-chain gene. Science (New York, N.Y 241, 1089–1092 (1988).
9. Jorgensen JL, Esser U, Fazekas de St Groth B, Reay PA & Davis MM Mapping T-cell receptor-peptide contacts by variant peptide immunization of single-chain transgenics. Nature 355, 224–230 (1992). [PubMed: 1309938]
10. Pacholczyk R, Ignatowicz H, Kraj P & Ignatowicz L Origin and T cell receptor diversity of Foxp3+CD4+CD25+ T cells. Immunity 25, 249–259 (2006). [PubMed: 16879995]
11. Wong J et al. Adaptation of TCR repertoires to self-peptides in regulatory and nonregulatory CD4+ T cells. J Immunol 178, 7032–7041 (2007). [PubMed: 17513752]
12. Beura LK et al. Normalizing the environment recapitulates adult human immune traits in laboratory mice. Nature 532, 512–516 (2016). [PubMed: 27096360]
13. Moran AE et al. T cell receptor signal strength in Treg and iNKT cell development demonstrated by a novel fluorescent reporter mouse. The Journal of experimental medicine 208, 1279–1289.
14. Moran AE et al. T cell receptor signal strength in Treg and iNKT cell development demonstrated by a novel fluorescent reporter mouse. The Journal of experimental medicine 208, 1279–1289 (2011). [PubMed: 21606508]
15. Howie D et al. MS4A4B is a GITR-associated membrane adapter, expressed by regulatory T cells, which modulates T cell activation. J Immunol 183, 4197–4204 (2009). [PubMed: 19752228]
16. Xing Y, Wang X, Jameson SC & Hogquist KA Late stages of T cell maturation in the thymus involve NF-kappaB and tonic type I interferon signaling. Nature immunology (2016).

17. Boursalian TE, Golob J, Soper DM, Cooper CJ & Fink PJ Continued maturation of thymic emigrants in the periphery. Nature immunology 5, 418–425 (2004). [PubMed: 14991052]
18. McCaughtry TM, Wilken MS & Hogquist KA Thymic emigration revisited. The Journal of experimental medicine 204, 2513–2520 (2007). [PubMed: 17908937]
19. Zhan Y, Bourges D, Dromey JA, Harrison LC & Lew AM The origin of thymic CD4+CD25+ regulatory T cells and their co-stimulatory requirements are determined after elimination of recirculating peripheral CD4+ cells. International immunology 19, 455–463 (2007). [PubMed: 17314081]
20. Paessens LC, Singh SK, Fernandes RJ & van Kooyk Y Vascular cell adhesion molecule-1 (VCAM-1) and intercellular adhesion molecule-1 (ICAM-1) provide co-stimulation in positive selection along with survival of selected thymocytes. Mol Immunol 45, 42–48 (2008). [PubMed: 17604837]
21. Gerner MY, Kastenmuller W, Ifrim I, Kabat J & Germain RN Histo-cytometry: a method for highly multiplex quantitative tissue imaging analysis applied to dendritic cell subset microanatomy in lymph nodes. Immunity 37, 364–376 (2012). [PubMed: 22863836]
22. Fontenot JD et al. Regulatory T cell lineage specification by the forkhead transcription factor foxp3. Immunity 22, 329–341 (2005). [PubMed: 15780990]
23. Bettini ML et al. Loss of epigenetic modification driven by the Foxp3 transcription factor leads to regulatory T cell insufficiency. Immunity 36, 717–730 (2012). [PubMed: 22579476]
24. Darce J et al. An N-terminal mutation of the Foxp3 transcription factor alleviates arthritis but exacerbates diabetes. Immunity 36, 731–741 (2012). [PubMed: 22579475]
25. Zheng Y et al. Role of conserved non-coding DNA elements in the Foxp3 gene in regulatory T-cell fate. Nature 463, 808–812 (2010). [PubMed: 20072126]
26. Feng Y et al. A mechanism for expansion of regulatory T-cell repertoire and its role in self-tolerance. Nature 528, 132–136 (2015). [PubMed: 26605529]
27. Huang H et al. Fine-mapping inflammatory bowel disease loci to single-variant resolution. Nature 547, 173–178 (2017). [PubMed: 28658209]
28. Huang J, Ellinghaus D, Franke A, Howie B & Li Y 1000 Genomes-based imputation identifies novel and refined associations for the Wellcome Trust Case Control Consortium phase 1 Data. Eur J Hum Genet 20, 801–805 (2012). [PubMed: 22293688]
29. Onengut-Gumuscu S et al. Fine mapping of type 1 diabetes susceptibility loci and evidence for colocalization of causal variants with lymphoid gene enhancers. Nature genetics 47, 381–386 (2015). [PubMed: 25751624]
30. Simeonov DR et al. Discovery of stimulation-responsive immune enhancers with CRISPR activation. Nature 549, 111–115 (2017). [PubMed: 28854172]
31. Schaeffer EM et al. Tec family kinases modulate thresholds for thymocyte development and selection. The Journal of experimental medicine 192, 987–1000 (2000). [PubMed: 11015440]
32. Huang W, Jeong AR, Kannan AK, Huang L & August A IL-2-inducible T cell kinase tunes T regulatory cell development and is required for suppressive function. J Immunol 193, 2267–2272 (2014). [PubMed: 25063868]
33. Wu JN et al. Adhesion- and degranulation-promoting adapter protein is required for efficient thymocyte development and selection. J Immunol 176, 6681–6689 (2006). [PubMed: 16709827]
34. Weinreich MA, Odumade OA, Jameson SC & Hogquist KA T cells expressing the transcription factor PLZF regulate the development of memory-like CD8+ T cells. Nature immunology 11, 709–716 (2010). [PubMed: 20601952]
35. Huang W, Huang F, Kannan AK, Hu J & August A ITK tunes IL-4-induced development of innate memory CD8+ T cells in a gammadelta T and invariant NKT cell-independent manner. J Leukoc Biol 96, 55–63 (2014). [PubMed: 24620029]
36. Burchill MA, Yang J, Vang KB & Farrar MA Interleukin-2 receptor signaling in regulatory T cell development and homeostasis. Immunol Lett 114, 1–8 (2007). [PubMed: 17936914]
37. Vang KB et al. IL-2, −7, and −15, but not thymic stromal lymphopoeitin, redundantly govern CD4+Foxp3+ regulatory T cell development. J Immunol 181, 3285–3290 (2008). [PubMed: 18714000]

38. Watanabe N et al. Hassall's corpuscles instruct dendritic cells to induce CD4+CD25+ regulatory T cells in human thymus. Nature 436, 1181–1185 (2005). [PubMed: 16121185]
39. Miller CN et al. Thymic tuft cells promote an IL-4-enriched medulla and shape thymocyte development. Nature 559, 627–631 (2018). [PubMed: 30022164]
40. Bornstein C et al. Single-cell mapping of the thymic stroma identifies IL-25-producing tuft epithelial cells. Nature 559, 622–626 (2018). [PubMed: 30022162]
41. Gerbe F et al. Intestinal epithelial tuft cells initiate type 2 mucosal immunity to helminth parasites. Nature 529, 226–230 (2016). [PubMed: 26762460]
42. McGeachy MJ, Stephens LA & Anderton SM Natural recovery and protection from autoimmune encephalomyelitis: contribution of CD4+CD25+ regulatory cells within the central nervous system. J Immunol 175, 3025–3032 (2005). [PubMed: 16116190]
43. Shahinian A et al. Differential T cell costimulatory requirements in CD28-deficient mice. Science (New York, N.Y 261, 609–612 (1993).
44. Sha WC, Liou HC, Tuomanen EI & Baltimore D Targeted disruption of the p50 subunit of NF-kappa B leads to multifocal defects in immune responses. Cell 80, 321–330 (1995). [PubMed: 7834752]
45. Liao XC & Littman DR Altered T cell receptor signaling and disrupted T cell development in mice lacking itk. Immunity 3, 757–769 (1995). [PubMed: 8777721]
46. Peterson EJ et al. Coupling of the TCR to integrin activation by Slap-130/Fyb. Science (New York, N.Y 293, 2263–2265 (2001).
47. Sonoda KH, Exley M, Snapper S, Balk SP & Stein-Streilein J CD1-reactive natural killer T cells are required for development of systemic tolerance through an immune-privileged site. The Journal of experimental medicine 190, 1215–1226 (1999). [PubMed: 10544194]
48. Shinkai Y et al. RAG-2-deficient mice lack mature lymphocytes owing to inability to initiate V(D)J rearrangement. Cell 68, 855–867 (1992). [PubMed: 1547487]
49. Nelson RW et al. T cell receptor cross-reactivity between similar foreign and self peptides influences naive cell population size and autoimmunity. Immunity 42, 95–107 (2015). [PubMed: 25601203]
50. Blair-Handon R, Mueller K & Hoogstraten-Miller S An alternative method for intrathymic injections in mice. Lab Anim (NY) 39, 248–252 (2010). [PubMed: 20664574]
51. Ruscher R, Kummer RL, Lee YJ, Jameson SC & Hogquist KA CD8alphaalpha intraepithelial lymphocytes arise from two main thymic precursors. Nature immunology 18, 771–779 (2017). [PubMed: 28530714]
52. Haribhai D et al. A requisite role for induced regulatory T cells in tolerance based on expanding antigen receptor diversity. Immunity 35, 109–122. [PubMed: 21723159]
53. Perry JS et al. Distinct contributions of Aire and antigen-presenting-cell subsets to the generation of self-tolerance in the thymus. Immunity 41, 414–426 (2014). [PubMed: 25220213]
54. Lin W et al. Regulatory T cell development in the absence of functional Foxp3. Nature immunology 8, 359–368 (2007). [PubMed: 17273171]
55. Spanier JA, Nashold FE, Mayne CG, Nelson CD & Hayes CE Vitamin D and estrogen synergy in Vdr-expressing CD4(+) T cells is essential to induce Helios(+)FoxP3(+) T cells and prevent autoimmune demyelinating disease. Journal of neuroimmunology 286, 48–58 (2015). [PubMed: 26298324]
56. Mottet C, Uhlig HH & Powrie F Cutting edge: cure of colitis by CD4+CD25+ regulatory T cells. J Immunol 170, 3939–3943 (2003). [PubMed: 12682220]

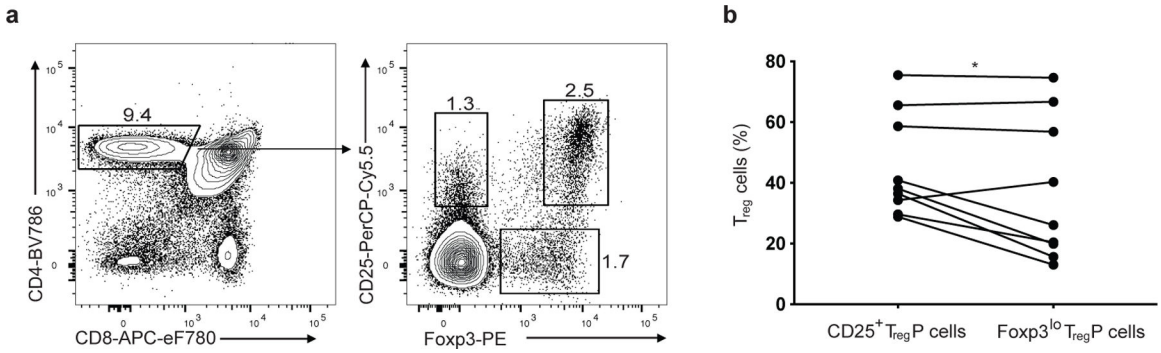

Figure 1.

Two thymic T_{reg} progenitor cell populations exist. a) Gating scheme used to quantify or isolate $CD25^{+}Foxp3^{-}$ and $CD25^{-}Foxp3^{lo}$ $T_{reg}P$ cell populations throughout the manuscript. b) Quantification of the proportion of sorted congenically distinct ($CD90.2^{+}CD45.2^{+}$ or $CD90.1^{+}CD45.2^{+}$) $CD25^{+}$ and $Foxp3^{lo}$ $T_{reg}P$ cells co-injected into the thymi of $CD45.1^{+}$ mice that differentiated into $CD25^{+}Foxp3^{+}$ T_{reg} cells 6 post-injection. Each dot represents a single recipient mouse; pairing represents data within the same recipient thymi. Data represents 3 independent experiments, n=9 mice. Data was analyzed by a two-sided paired *t* test. * $P<0.05$.

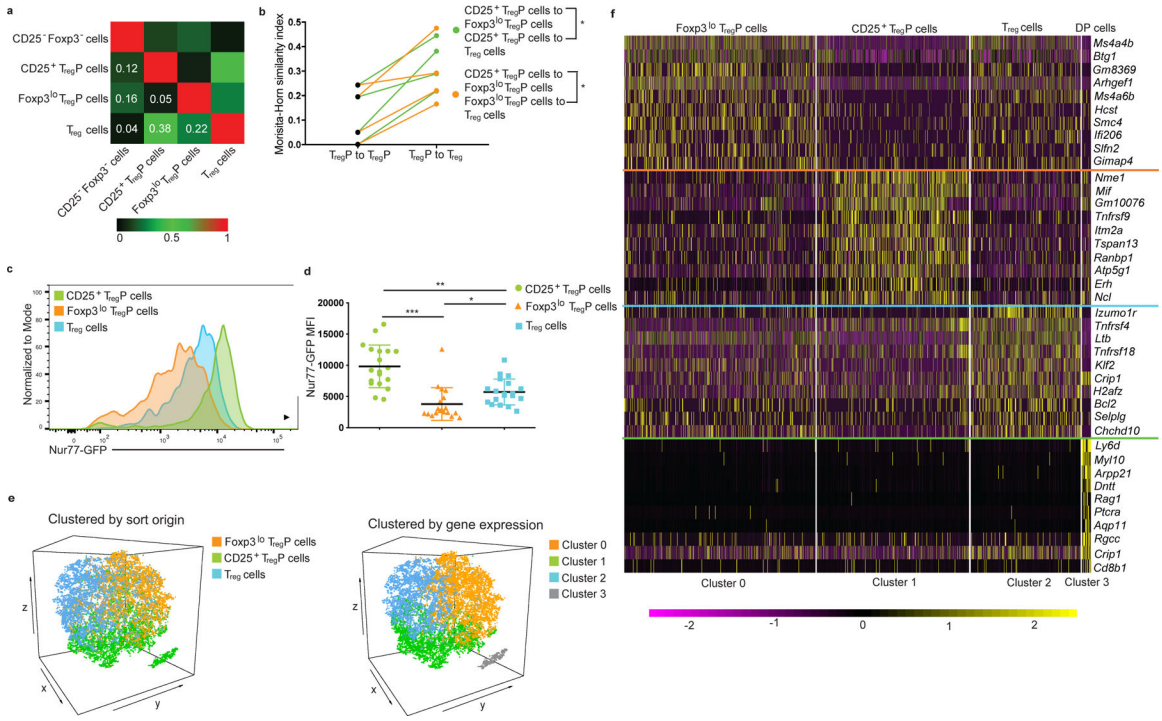

Figure 2.

CD25$^+$ and Foxp3^{lo} T$_{reg}$P are distinct thymic T$_{reg}$ cell lineages. a) Morisita-Horn indices comparing similarity of Vα2 CDR3 repertoires generated by TCR sequencing of CD4$^+$CD25$^-$Foxp3$^-$, CD4$^+$CD25$^+$Foxp3$^-$ T$_{reg}$P, CD4$^+$CD25$^-$Foxp3^{lo} T$_{reg}$P and CD4$^+$CD25$^+$Foxp3^{lo} mature T$_{reg}$ cells isolated from Tcliβ$^+$ *TCRa*$^{+/-}$ mice. b) Plot of the ratio of Morisita-Horn similarity indices comparing TCRs in CD25$^+$ and Foxp3^{lo} T$_{reg}$P cell populations, and TCRs in CD25$^+$T$_{reg}$P and mature T$_{reg}$ cells or Foxp3^{lo} T$_{reg}$P and mature T$_{reg}$ cells. CD25$^+$ T$_{reg}$P cell comparisons are shown in green and Foxp3^{lo} T$_{reg}$P cell comparisons are shown in orange. Data represents 2 independent experiments, n=4 mice. Data was analyzed by a two-sided paired *t* test. c,d) Flow cytomyerty analysis of Nur77-GFP MFI in CD25$^+$Foxp3$^-$ T$_{reg}$P, CD25$^-$Foxp3^{lo} TregP and CD25$^+$Foxp3$^+$ mature T$_{reg}$ cells obtained from thymi of Nur77-GFP reporter mice. Dots represent individual mice. Data are displayed as mean ± SD and represents 7 independent experiments, n=19 mice. Data was analyzed via a two-sided paired Friedman test with Dunn's multiple comparisons test. e) Left- Three-dimensional tSNE plots from 10X Genomics single-cell RNA-Seq data set for sorted CD25$^+$ T$_{reg}$P, Foxp3$_{lo}$ T$_{reg}$P and CD25$^+$Foxp3$^+$ T$_{reg}$ cells displaying relationships between individual cells with color-coding based on flow cytometry sort origin. Right- Three-dimensional tSNE plots of identical data to left panel but color-coded based on gene expression profiles. f) Heatmap for the top 10 differentially regulated genes from each cluster derived from subfigure e. Each column represents gene expression for an individual cell; yellow is up and purple is down. Data from e,f is representative of 3 independent experiments, n=3 mice. *P<0.05, **P<0.0005, ***P<0.0001.

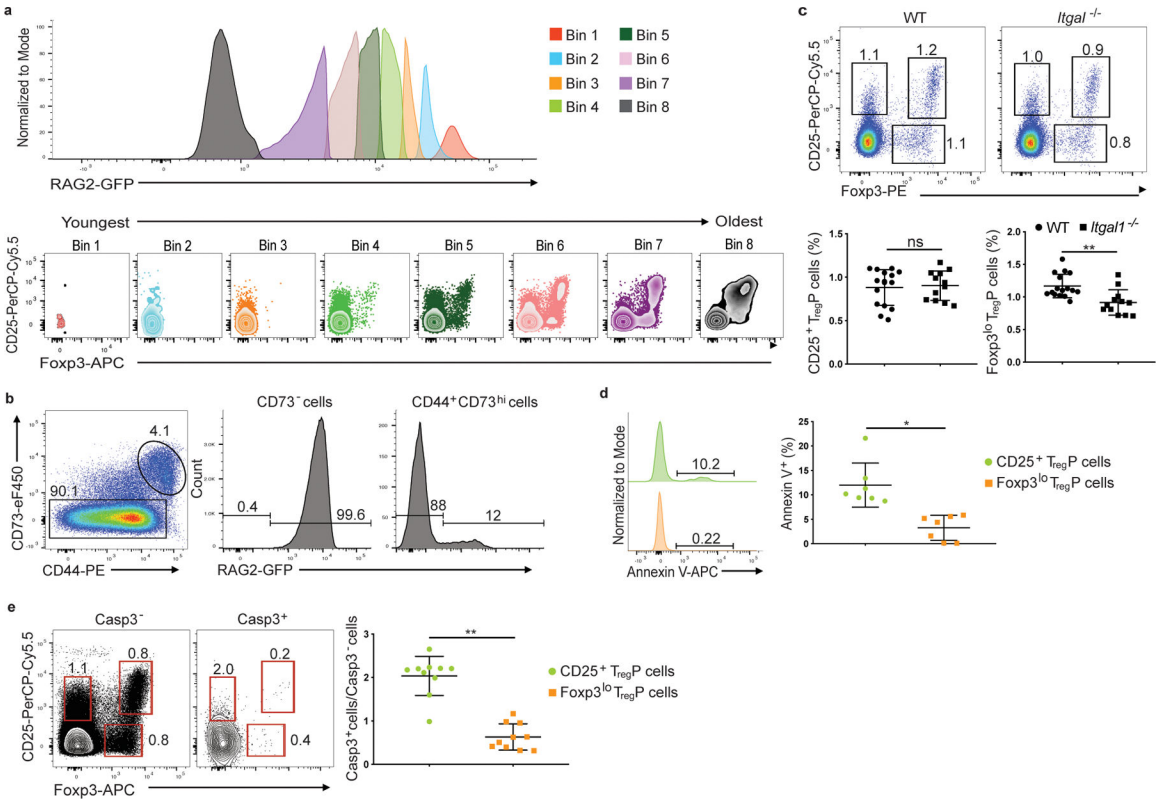

Figure 3.

$CD25^+$ and $Foxp3^{lo}$ $T_{reg}P$ cells are in discrete selection stages. a) Representative histograms of RAG2-GFP expression in CD4SP thymocytes obtained from thymi of RAG2-GFP mice. Bins are displayed from high (Bin 1) to low (Bin 8) RAG-GFP expression and cells in each bin are plotted for CD25 vs Foxp3 expression. Data shown are concatenated results from 3 mice and are representative of 7 independent experiments, n=9 mice. b) Representative flow cytometry plots of CD73 staining in CD4SP thymocytes and RAG2-GFP expression in $CD73^-$ and $CD73^+$ compartments. Data is representative of 5 experiments, n=5 mice. c) Representative flow cytometry plots (top) and quantification of the percent of $CD4^+CD73^-$ thymocytes differentiating into each $T_{reg}P$ cell population in WT versus *Itgal*$^{-/-}$ thymi. Data represents 3 independent experiments, n= 16 WT and *Itgal*$^{+/-}$ mice, n=12 *Itgal*$^{-/-}$ mice. Data was analyzed by two-sided Mann-Whitney test. d) Left panels, Representative example of Annexin V expression on $CD4^+CD73^-CD25^+Foxp3^-$ $T_{reg}P$ (top green histogram) and $CD4^+CD73^-CD25^-Foxp3^{lo}$ $T_{reg}P$ (bottom orange histogram) thymocytes from *Foxp3-GFP* mice. Right panel, quantification of Annexin V staining on $CD25^+$ $T_{reg}P$ and $Foxp3_{lo}$ $T_{reg}P$. Data represents 3 independent experiments, n=9 mice. Data were analyzed by two-sided Wilcoxon matched-pairs signed rank test. e) Left and middle panels, represenative examples of staining for CD25 and Foxp3 on $CD4^+CD73^-$ gated thymocytes from wild-type mice either negative (left panel) or positive (middle panel) for cleaved caspase-3. Right panel, quantification of the ratio of cleaved caspase-3-positive to cleaved caspase-3 negative $CD25^+$ $T_{reg}P$ (green circles) or Foxp3lo $T_{reg}P$; data represents 4 independent experiments, n=10 mice. Data were analyzed by two-sided Wilcoxon matched-pairs signed rank test. All data are displayed as mean ± SD. *P<0.05, **P<0.005, ns-not significant.

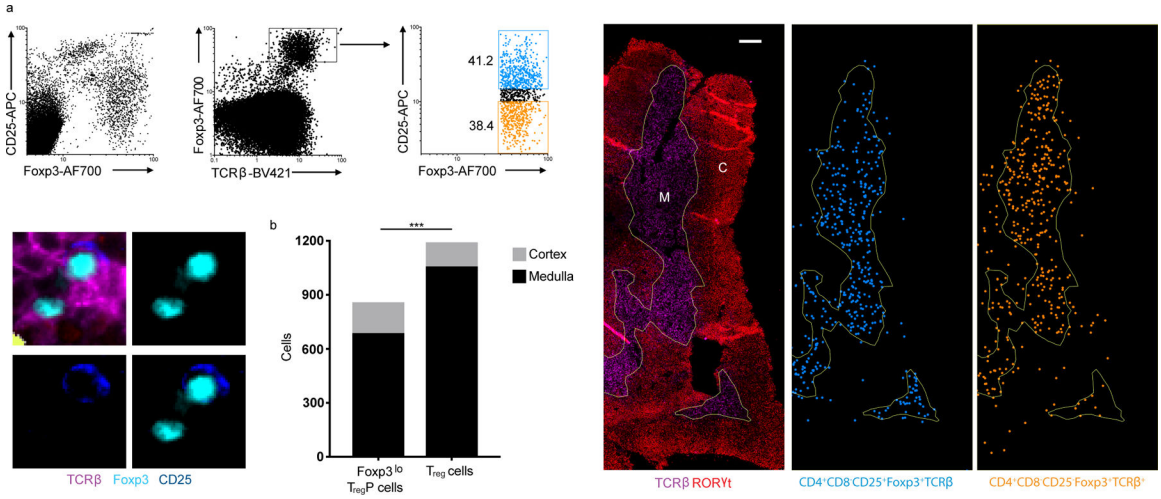

Figure 4.

T_{reg} cells and Foxp3^{lo} T_{reg}P cells show different localization in the thymus. a) Top left panels, representative histocytometry dot plots of thymocytes stained with antibodies to CD25, Foxp3 and TCRβ used to denote Foxp3^{lo} T_{reg}P cells (CD25^{-}Foxp3^{+}TCRβ^{+}) and T_{reg} cells (CD25^{+}Foxp3^{+}TCRβ^{+}) within stained thymic sections. Bottom left panels, representative images of Foxp3^{lo} T_{reg}P cells and T_{reg} cells. Right panels, thymic sections stained with antibodies to TCRb and RORgt used to delineate the thymic medulla (M) and cortex (C). Distribution of CD25^{+}Foxp3^{+}TCRβ^{+} T_{reg} cells (blue) and CD25^{-}Foxp3^{+}TCRβ^{+} Foxp3^{lo} T_{reg}P cells (orange) within the thymic medulla and cortex (right). Scale bar represents 200μm. b) Distribution of Foxp3^{lo} T_{reg}P cells and T_{reg} cells between thymic cortex and medulla, p value determined by Fisher's exact test. Data represents 1 experiment, n=2 mice. ***P<0.0001.

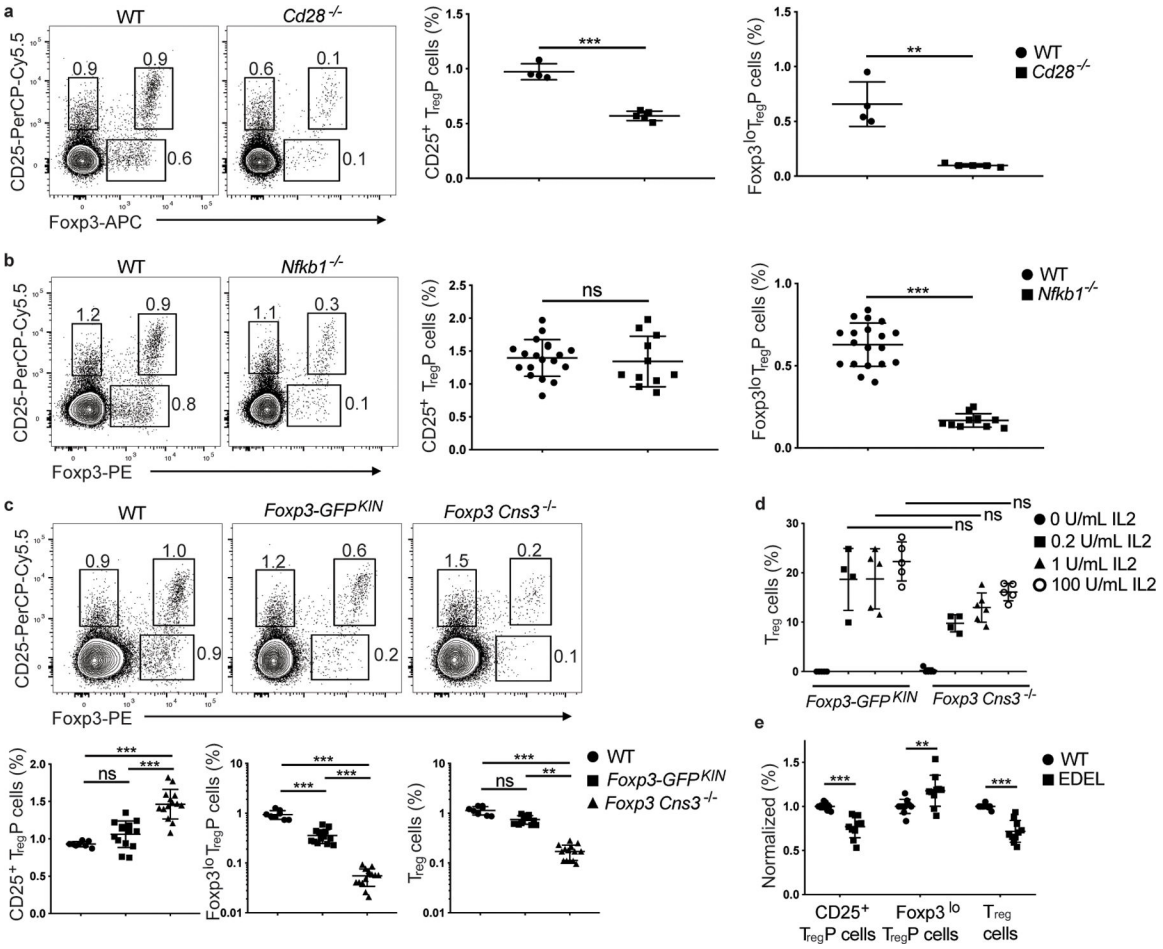

Figure 5.

Foxp3^{lo} T$_{reg}$P cells are dependent on NFκB1 activation and the Foxp3 regulatory element *Cns3*. a), Left panels, shown are representative flow cytometry plots for CD4^{+}CD8^{-}CD73^{-} gated thymocytes antibodies from wild-type and *Cd28*$^{-/-}$ mice stained with antibodies to CD25 and Foxp3 (1 experiment, n=4 wild-type and 5 *Cd28*$^{-/-}$ mice). Right panels show cumulative data for all mice and depict the relative percentage of CD25^{+} T$_{reg}$P and Foxp3^{lo} T$_{reg}$P in CD4^{+}CD8^{-}CD73^{-} thymocytes from wild-type and *Cd28*$^{-/-}$ mice. b), Shown are representative flow cytometry plots for CD4^{+}CD8^{-}CD73^{-} gated thymocytes from wild-type and *Nfkb1*$^{-/-}$ mice stained with antibodies to CD25 and Foxp3 (3 independent experiments, n=19 wild-type and 11 *Nfkb1*$^{-/-}$ mice). Right panels show cumulative data for all mice and depict the relative percentage of CD25^{+} T$_{reg}$P and Foxp3^{lo} T$_{reg}$P in CD4^{+}CD8^{-}CD73^{-} thymocytes from wild-type and *Nfkb1*$^{-/-}$ mice c) Top panels, shown are representative flow cytometry plots for CD4^{+}CD8^{-}CD73^{-} gated thymocytes from wild-type, FOXP3-GFP^{KIN}, and *Cns3*$^{-/-}$ mice stained with antibodies to CD25 and Foxp3 (4 independent experiments, n=8 wild-type, 14 Foxp3-GFP^{KIN}, and 14 *Cns3*$^{-/-}$ mice). Right panels show quantification of cumulative data for all mice and depict relative percentage of CD25^{+} T$_{reg}$P and Foxp3^{lo} T$_{reg}$P in CD4^{+}CD8^{-}CD73^{-} thymocytes from wild-type (black circles), Foxp3-GFP^{KIN} (black squares), and *Cns3*$^{-/-}$ (black triangles) mice. d) Shown are the percentages of CD25^{+}Foxp3^{+} mature T$_{reg}$ cells generated after stimulating sorted CD4^{+}CD8^{-}CD73^{-}CD25^{+}

$T_{reg}P$ cells from thymi of Foxp3-GFP^{KIN} and *Cns3*$^{-/-}$ mice for 3 days with 0 U/ml IL2 (black circles, n=5 Foxp3-GFP^{KIN} and 5 *Cns3*$^{-/-}$ mice), 0.2 U/ml IL2 (black squares, n=4 Foxp3-GFP^{KIN} and 5 *Cns3*$^{-/-}$ mice), 1 U/ml IL2 (black triangles, n=5 Foxp3-GFP^{KIN} and 6 *Cns3*$^{-/-}$ mice) and 100 U/ml (open circles, n= Foxp3-GFP^{KIN} and 5 *Cns3*$^{-/-}$ mice) and come from 2 independent experiments. e) Quantification of cumulative data from 2 independent experiments showing the relative percentage of CD25^{+} $T_{reg}P$, Foxp3^{lo} $T_{reg}P$ and mature CD25^{+}Foxp3^{+} T_{reg} cells from CD4^{+}CD8^{-}CD73^{-} gated thymocytes from wild-type (black circles) or EDEL mice, which lack the CaRE4 enhancer (black squares). Data represents 2 independent experiments, n=10 wild-type and 10 EDEL mice. a,b) Data was analyzed by two-sided unpaired *t* test. c) CD25^{+} $T_{reg}P$ cells (%) and Foxp3^{lo} $T_{reg}P$ cells (%) were analyzed by one-way ANOVA with Tukey's multiple comparison test and T_{reg} cells (%) was analyzed by Kruskal-Wallis test with Dunn's multiple comparison test. d) Data was analyzed by Kruskal-Wallis test with Dunn's multiple comparisons test. e) Data was analyzed by two-way ANOVA with Sidak multiple comparisons test. All data are displayed as mean ± standard deviation. **P<0.005, ***P<0.0001, ns- not significant.

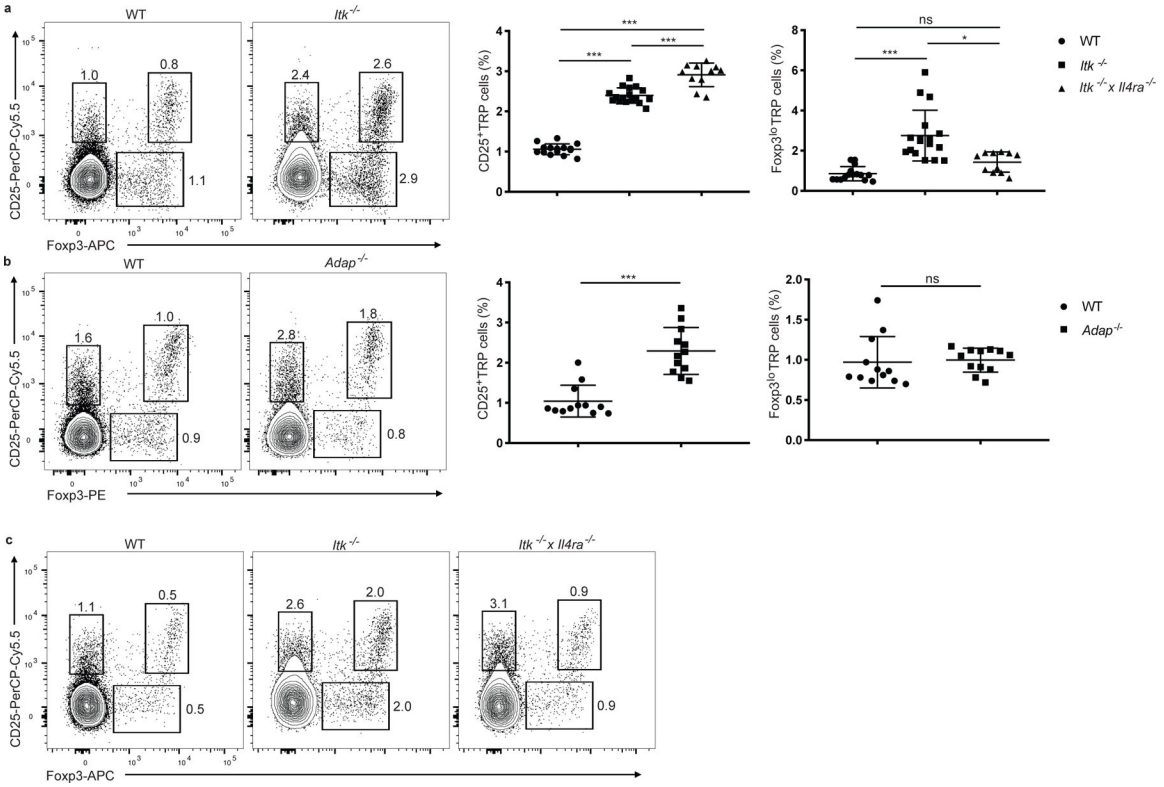

Figure 6.

Itk$^{-/-}$ mice have increased T_{reg} cell production from both $T_{reg}P$ cell pathways via distinct molecular mechanisms. a) Left panels, representative flow cytometry plots of $CD4^+CD8^-CD73^-$ gated thymocytes from wild-type versus *Itk*$^{-/-}$ mice stained with antibodies to CD25 and FOXP3. Right panels show cumulative data for all mice and depict the relative percentage of $CD25^+$ $T_{reg}P$ and $Foxp3^{lo}$ $T_{reg}P$ in $CD4^+CD8^-CD73^-$ thymocytes from wild-type, *Itk*$^{-/-}$, and *Itk*$^{-/-}$ *x Il4ra*$^{-/-}$mice (3 independent experiments, n=15 wild-type, 17 *Itk*$^{-/-}$ mice, and 11 *Itk*$^{-/-}$ *x Il4ra*$^{-/-}$). b) Left panels, representative flow cytometry plots of $CD4^+CD8^-CD73^-$ gated thymocytes from wild-type versus *Adap*$^{-/-}$ mice stained with antibodies to CD25 and FOXP3. Right panels show cumulative data for all mice and depict the relative percentage of $CD25^+$ $T_{reg}P$ and $Foxp3^{lo}$ $T_{reg}P$ in $CD4^+CD8^-CD73^-$ thymocytes from wild-type, and *Adap*$^{-/-}$mice (3 independent experiments, n=12 wild-type and 12 *Adap*$^{-/-}$ mice). c) .representative flow cytometry plots of $CD4^+CD8^-CD73^-$ gated thymocytes from wild-type, *Itk*$^{-/-}$ and *Itk*$^{-/-}$ *x Il4ra*$^{-/-}$mice stained with antibodies to CD25 and FOXP3. a) $CD25^+$ $T_{reg}P$ cell (%) was analyzed by one-way ANOVA with Tukey's multiple comparisons test; $Foxp3^{lo}$ $T_{reg}P$ cells (%) was analyzed by Kruskal-Wallis with Dunn's multiple comparisons test. b) Data was analyzed by two-sided Mann-Whitney test. All data are displayed as mean ± SD. *P<0.05, ***P<0.0001, ns-not significant.

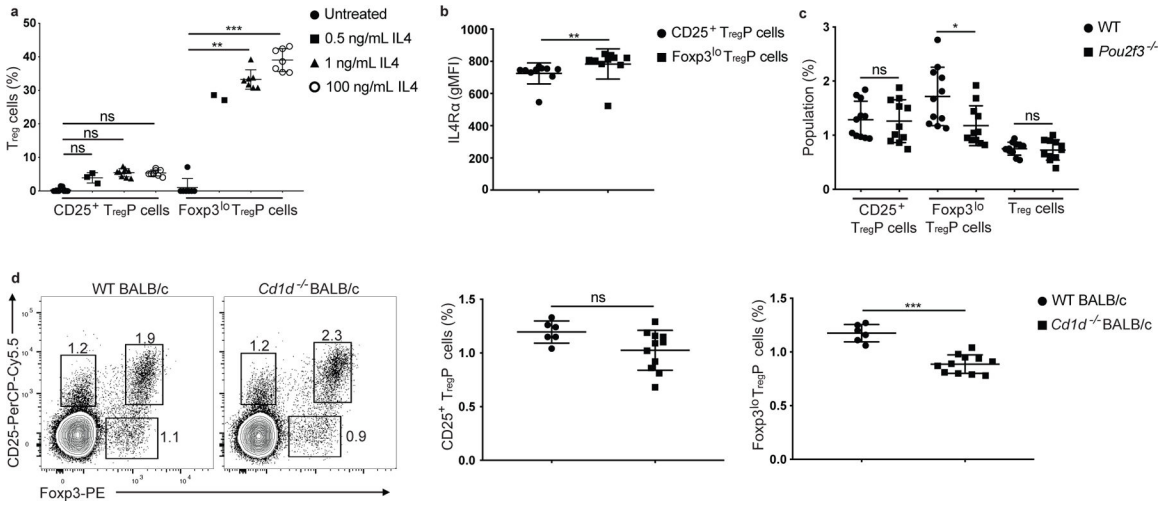

Figure 7.

CD25$^+$ and Foxp3^{lo} T_{reg}P cells have distinct cytokine responsiveness. a) Percent of T_{reg} cells generated from sorted CD4$^+$CD8$^-$CD73$^-$CD25$^+$FOXP3$^-$ and CD4$^+$CD8$^-$CD73$^-$CD25$^+$FOXP3$^-$ T_{reg}P cell subsets stimulated for 3 days with no cytokine (black circles, n=9 CD25$^+$ T_{reg}P and 7 Foxp3^{lo} T_{reg}P cultures), 0.5 ng/ml IL4 (black squares, n= 3 CD25$^+$ T_{reg}P and 2 Foxp3^{lo} T_{reg}P cultures), 1 ng/ml IL4 (black triangles, n= 9 CD25$^+$ T_{reg}P and 7 Foxp3^{lo} T_{reg}P cultures), and 100 ng/ml IL4 (open circles, n= 9 CD25$^+$ T_{reg}P and 7 Foxp3^{lo} T_{reg}P cultures) . Data is representative of 3 independent experiments (excluding 0.5 ng/mL IL4 stimulation which is from 1 experiment) and was analyzed by Kruskal-Wallis test with Dunn's multiple comparisons test. b) IL4Ra gMFI in CD25$^+$ (black circles) and Foxp3^{lo} (black squares) T_{reg}P cells from thymi of wild-type mice. Data is representative of 2 independent experiments, n=10 mice. Data analyzed by two-sided Wilcoxon matched-pairs signed rank test. c) Percent of CD4$^+$CD8$^-$CD73$^-$CD25$^+$Foxp3$^-$ T_{reg}P, CD4$^+$CD8$^-$CD73$^-$CD25$^-$Foxp3^{lo} T_{reg}P, and CD4$^+$CD8$^-$CD73$^-$CD25$^+$Foxp3$^+$ T_{reg} cells in thymi from wild-type (black circles, n=11 mice) and *Pou2f3*$^{-/-}$ mice (black squares, n= 11 mice). Data is representative of 2 independent experiments, and was analyzed by a two-sided unpaired *t* test. d) Left panels, representative flow cytometry plots of CD4$^+$CD8$^-$CD73$^-$ gated thymocytes from wildtype BALB/c and *Cd1d*$^{-/-}$ BALB/c mice stained with antibodies to CD25 and Foxp3. Right panels, percent of CD4$^+$CD8$^-$CD73$^-$CD25$^+$Foxp3$^-$ T_{reg}P (left) and CD4$^+$CD8$^-$CD73$^-$CD25$^-$Foxp3^{lo} T_{reg}P (right) in wild-type Balb/c (back circles) and Cd1d−/− Balb/c (black squares) mice. Data is representative of 2 independent experiments, n=6 mice-WT and 11 mice-*Cd1d*$^{-/-}$ and was analyzed by two-sided unpaired t-test. All data are displayed as mean ± SD. *P<0.05, **P<0.005, ***P<0.0001, ns-not significant.

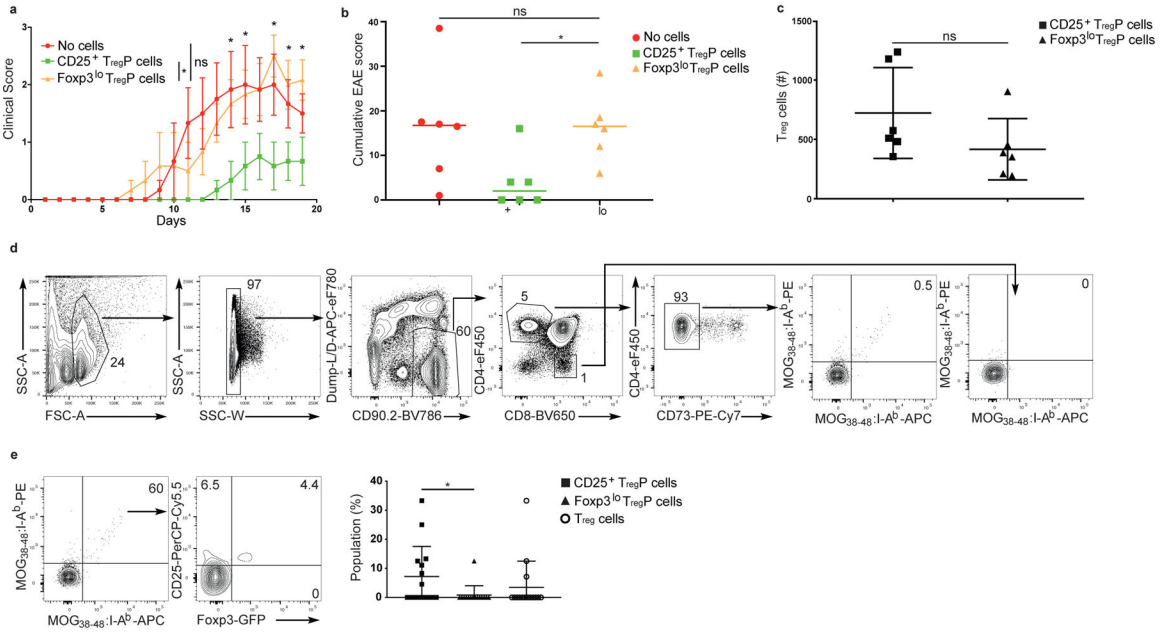

Figure 8.

$CD25^+$ and $Foxp3^{lo}$ $T_{reg}P$ cells are functionally distinct. a) Clinical score over 20-day time course of $MOG_{35–55}$ peptide-induced experimental autoimmune encephalomyelitis in wild-type mice treated with no T_{reg} cells (red line and circles), $Foxp3^{lo}$ $T_{reg}P$ (orange line and circles) and CD25+ $T_{reg}P$ (green lines and circles). Data was analyzed by two-sided unpaired t-tests with Holm-Sidak multiple comparisons correction. Asterisks mark values with adjusted p-values less than 0.05. Bars represent mean ± SEM. b) Cumulative EAE scores for control mice (no treatment, red circles), or mice injected with CD25+ $T_{reg}P$ (green squares) or $Foxp3^{lo}$ $T_{reg}P$ (yellow triangles). Data was analyzed by Kruskal-Wallis test with Dunn's multiple comparisons test. Bar represents median. c) Number of donor T_{reg} cells recovered from the spleen of EAE-induced mice receiving $CD25^+$ $T_{reg}P$ (black squares) and $Foxp3^{lo}$ $T_{reg}P$ (black triangles). Data was analyzed by a two-sided unpaired *t* test. Bars represent mean ± SD. a-c) Data represent 2 independent experiments, n=6 mice per group. d) Representative gating strategy for thymic tetramer pulldowns. Dual tetramer gates are drawn on $CD8^+$ thymocytes such that ~0% of $CD8^+$ thymocytes appear in the double tetramer positive gate. This gate is applied to $CD4^+CD73^-$ thymocytes to identify bona fide $MOG_{38–48}$:$I\text{-}A^b$ specific thymocytes. e) Representative flow cytometry plots of MOG tetramer pulldowns, concatenated from 6 thymi from wild-type mice. Left plot, number of MOG:$I\text{-}A^b$ dual-tetramer$^+$ T cells within the $CD4^+CD73^-$ thymocyte cell gate. Middle plot, percentage of MOG:$I\text{-}A^b$ dual tetramer$^+$ cells in $CD25^+T_{reg}P$ cell, $Foxp3^{lo}$ $T_{reg}P$ cell and T_{reg} cell gates. Right plot, cumulative data showing percentage of percentage of $CD25^+$ $T_{reg}P$ cells (black squares), $Foxp3^{lo}$ $T_{reg}P$ cells (black triangles), and Treg cells (open circles) in thymi from 15 wild-type mice. Data was analyzed by two-sided Wilcoxon matched-pairs signed rank test and is pooled from 3 independent experiments. Bars represent mean ± SD. *P<0.05, ns-not significant.

Table 1:

List of representative TCR Vα2 CDR3 sequences and the relative read distribution in each sorted population (conventional defined as $CD4^+CD8^-CD25^-Foxp3^-$).

Amino acid sequence	Reads Conventional	Read $CD25^+$ T_{reg}P cells	Reads $Foxp3^{lo}$ T_{reg}P cells	Reads T_{reg} cells
CAASGSAGNKLTF	0	0	2737	7714
CAAKSGSFNKLTF	0	1888	0	3587
CAAKHSGTYQRF	0	0	1176	3093
CAAPSSGSWQLIF	0	2028	659	1697
CAASYYNQGKLIF	0	349	0	1801
CAASKGSNYQLIW	0	569	0	1729
CAASAPYNQGKLIF	0	0	4221	1428
CAASSSGSFNKLTF	0	0	1392	1399
CAASLDYSNNRLTL	0	1015	863	1097
CAARASGSWQLIF	0	224	1044	2080
CAAASSGSWQLIF	0	432	268	1177
CAARNYNQGKLIF	1092	5278	2532	7041
CAASGTGGYKVVF	199	317	2870	1128